Surface Science Study of Water and Hydrogen Adsorbed on Rutile TiO_2(110)-(1×1)

Ke Cao

Liuzhou, China

Bachelor of Science, Peking University, 2011

A Thesis presented to the Graduate Faculty

of the University of Virginia in Candidacy for the Degree of

Master of Science

Department of Chemistry

University of Virginia

January, 2014

ABSTRACT

The dissociative adsorption of water at oxygen-vacancy defect sites on the TiO_2(110) surface spatially redistributes the defect electron density originally present at subsurface sites near the defect sites. This redistribution of defect-electrons makes them more accessible to Ti^{4+} ions surrounding the defects. The redistribution of electron density decreases the O^+ desorption yield from surface lattice O^{2-} ions in TiO_2, as excited by electron stimulated desorption (ESD). A model in which OH formation on defect sites redistributes defect electrons to neighboring Ti^{4+} sites is proposed. This switches off the Knotek-Feibelman mechanism for ESD of O^+ ions from lattice sites. Conversely, enhanced O^+ reneutralization could also be induced by redistribution of defect electrons. The redistribution of surface electrons by adsorption is further verified by the use of donor and acceptor molecules which add or remove electron density.

We have found a new form of chemically-bound hydrogen on the TiO_2(110) surface (H/TiO_2), which is produced by exposure to atomic H at 87 K. This chemisorbed hydrogen differs significantly in its physical properties from OH/TiO_2 produced by H_2O adsorption. The H/TiO_2 species produces a normal beam of H^+ upon electron stimulated desorption whereas OH/TiO_2 species produce inclined H^+ ESD beams. An inclined O-H bond in OH/TiO_2 results in an elliptic H^+ ion angular distribution pattern. H/TiO_2 is thermally less stable than OH/TiO_2. By ~ 350 K, H/TiO_2 has disappeared, probably by thermal

desorption or diffusion into the bulk, whereas OH/TiO_2 begins to desorb as H_2O only above ~350 K.

ACKNOWLEGMENTS

I sincerely thank my advisor, Prof. John T. Yates, Jr. for his intellectual support and continual encouragement through my studies. This thesis was made possible by his patience and persistence. John has very rich knowledge and experience in teaching physical chemistry and surface science research. I was deeply inspired by his active involvement in class as well as his critical and rigorous spirit in scientific research.

I thank Dr. Zhen Zhang for his continual support and teaching me all the ultra-high vacuum system operation skills, as well as his help in my daily life. His rich knowledge and experience in surface science study impressed me and I learned very much from him.

I am grateful to Prof. Ion Harrison, who gave me good suggestions when I encountered problems. I would like to thank Prof. Kevin K. Lehmann, Prof. Eric Herbst, Prof. Sergei A. Egorov and Prof. Petra Reinke, for their excellence in teaching me profound knowledge in chemistry and materials.

I also wish to thank my lab mates, including Dr. Michael Büttner, Dr. Mahesh Rajappan, Dr. Isabel Green, Dr. Lynn Mandeltort, Ana Stevanovic, Chunqing Yuan, Monica McEntee and Shiliang Ma, for their help in the laboratory as the coworkers.

I am also thankful to Prof. David H. Metcalf, who provided help with ultraviolet test of filters in his course lab.

I want to thank my parents and my sister for their support of my studying abroad. Their encouragement and support drives me forward all the time.

Finally, full support for the project from DOE, Office of Basic Energy Science, under grant number DE-FG02-O9ER16080 is gratefully acknowledged.

Table of Contents

CHAPTER ONE: Introduction

1.1 TiO_2 Applications and TiO_2(110) Surface

Titanium dioxide (TiO_2) is one of the most promising semiconductor materials in diverse applications. Notably, the discovery of photocatalytic splitting of water on TiO_2 electrodes by Fujishima and Honda in 1972 started a new era of TiO_2 study[1]. In 1991, O'Regan and Gratzel first reported nanocrystalline TiO_2 dye-sensitized solar cell (DSSC) with an efficiency of 7.1-7.9% under simulated solar light[2], which was another milestone in the history of research of TiO_2. Besides photocatalytic water splitting and DSSC, TiO_2 has sparked extensive research interests, including photocatalytic degradation of organic polluntants[3], gas sensors[4-5], self-cleaning coating[6], and UV-induced hydrophilicity[7].

1.1.1 Rutile TiO_2(110) Structure

Titanium dioxide exists mainly in three phases in nature: anatase, rutile and brookite. The lattice structure of anatase and rutile TiO_2 is shown in Figure 1.1, and brookite is not used often in research. Both of the structures of rutile and anatase can be described in terms of distorted TiO_6 octahedra chains. The octahedron in rutile shows a slight orthorhombic distortion, while in anatase, the octahedron is significantly distorted and has a lower symmetry than orthorhombic[8].

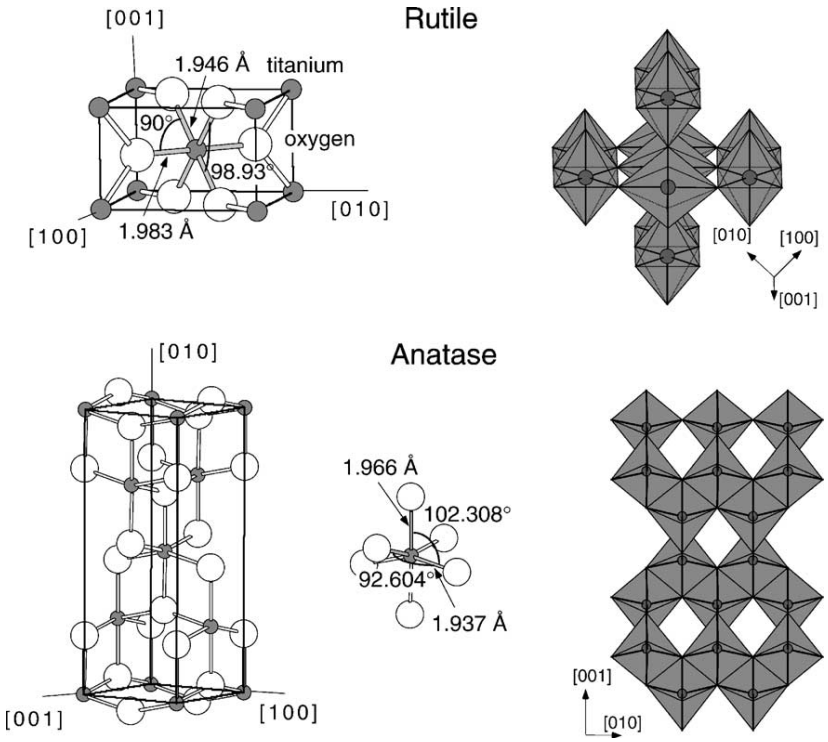

Figure 1.1: Lattice structure of rutile and anatase TiO_2, showing bond lengths and bond angles. Figure is reproduced from Reference[9].

Crystalline rutile has three low-index faces, (110), (100) and (001). A diagram of these faces is shown in Figure 1.2. Among them, (110) is the most thermally stable face and thus the most studied.

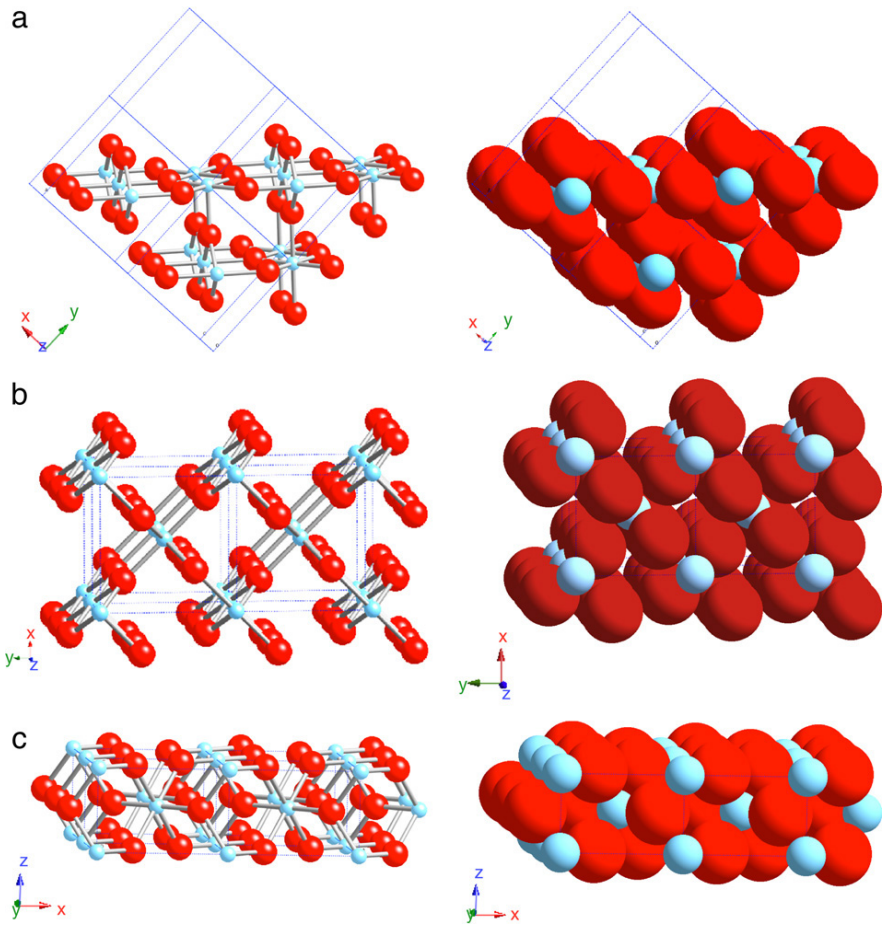

Figure 1.2: Schematic diagram of faces of rutile: (a)(110); (b)(100); (c)(001). Figure is reproduced from Reference[10].

1.1.1.1 TiO_2(110)-(1×1)

The rutile TiO_2(110)-(1×1) surface with some known point defects is shown in Figure 1.3. The surface contains rows of bridge-bonded oxygen (BBO) atoms that lie above the in-plane surface. Bridge-bonded oxygen vacancy (BBOV) sites are usually generated by sputtering and annealing[9]. The BBO rows are located on top of 6-fold coordinated Ti (Ti_{6c})

rows, which are in the same plane as 5-fold coordinated (Ti_{5c}) rows. The rows of in-plane oxygen atoms separate Ti_{5c} and Ti_{6c} rows.

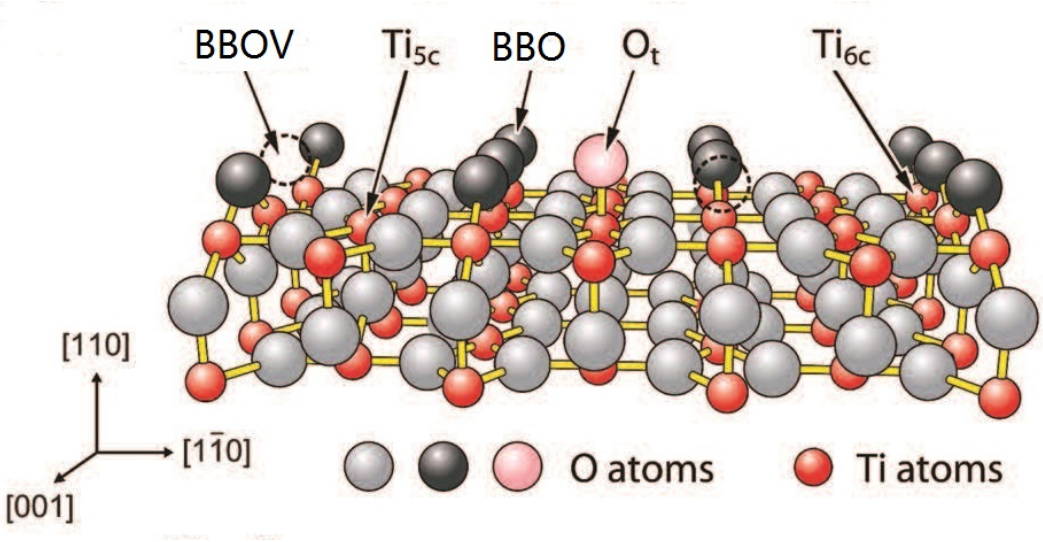

Figure 1.3: Ball-and-stick model of rutile TiO_2(110)-(1×1) surface with some point defects. Figure is modified from Reference[11].

1.1.1.2 TiO_2(110)-(1×2)

A TiO_2(110)-(1×2) surface is the most common observed reconstruction on rutile TiO_2(110), which is caused by annealing of a reduced TiO_2(110) at high temperature (748-998 K)[12]. The structure of (1×2) (Figure 1.4) can be described as alternate BBO rows are absent from the regular (1×1) surface. We kept the annealing temperature below 950 K to avoid the the reconstruction from (1×1) to (1×2) and the (1×1) structure is testified by LEED in our experiments.

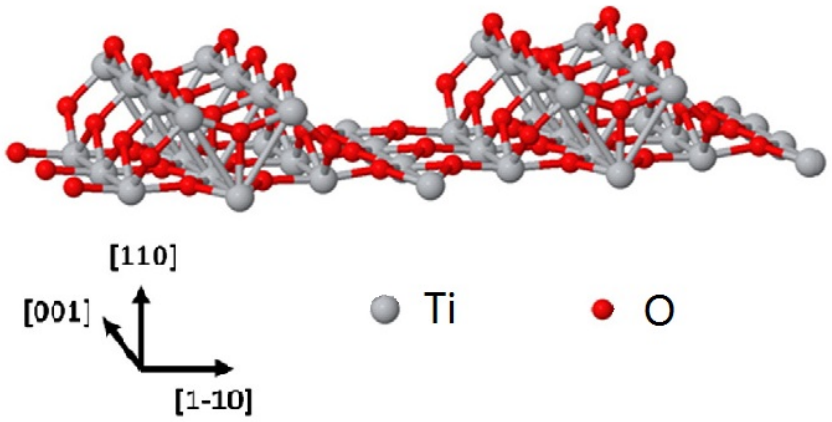

Figure 1.4: Ball-and-stick model of rutile TiO_2(110)-(1x2). Figure is modified from Reference[13].

1.2 Previous Study of Water and Hydrogen Adsorbed on TiO_2(110)

1.2.1 Water on TiO_2(110)

Water is probably considered the most important adsorbate on TiO_2 and is widely studied, since water is present in virtually all TiO_2 technological applications. Specifically on TiO_2(110), it is well established that adsorbed H_2O dissociates at BBOV sites and forms one OH (called BBOH) species at the vacancy site, and another H atom sits on a nearby BBO, forming another BBOH, as shown in Figure 1.5. Low temperature STM[14] and high-resolution electron energy loss spectroscopy (HREELS)[15] studies indicated that the dissociation of water can occur as low as ~187 K. Two BBOHs recombine when heated to ~490 K, forming a H_2O(g) molecule and regenerating a BBOV site[16-17]. The oxygen isotope exchange experiments showed that BBOHs can

diffuse to other BBO sites[16]. A typical TPD spectrum of H_2O on TiO_2(110) is shown in Figure 1.6[18], in which the three peaks, 163 K, 265 K, and 490 K, are attributed to multilayer water desorption, H_2O desorption from Ti_{5c}, and recombination of two BBOH species, respectively. The product of water dissociative adsorption, BBOH, plays an important role in many aspects of catalysis on TiO_2, including facilitating the adsorption of O_2 on TiO_2(110)[19], the exothermic reaction of CO_2 and H_2O to form bicarbonate species[20] and the binding of NO on TiO_2(110)[21]. Therefore, researchers are interested in its diffusion properties. STM studies of BBOH species elucidated that BBOH pairs diffuse along the $[1\bar{1}0]$ direction through proton exchange with H_2O[14] and hop along the [001] direction[22]. It was also found that the two BBOHs, resulting from one H_2O molecule dissociation at one BBOV site, are not equivalent by STM studies[22]. Besides monolayer water, multilayer water on TiO_2(110) also attracts researchers' interest. The first layer of H_2O, corresponding to the ~265 K peak, is absorbed on Ti_{5c} sites with O atom pointing to Ti_{5c}. This model was confirmed by a work function study[23] and STM images[14, 24-26]. After water molecules fill the Ti_{5c} sites, a second layer (or more layers) of water adsorbs over BBO rows, corresponding to the ~175 K (~163 K) TPD peak. Structures of multilayer water are debated. A work function study suggested that the second layer water sits parallel to the surface[23]. HREELS results showed that hydrogen bond exists within the second layer, not between the first and second layers[27].

Nevertheless, H-D exchange experiments showed the second layer of water hydrogen bonds to the first layer[28]. Recently, Lee et al. found that water molecules can form H-bonded one-dimensional chains at high water coverage on TiO_2(110), through STM measurements and DFT calculations, which provided insight into nature of H-bonding in wetting of TiO_2[29].

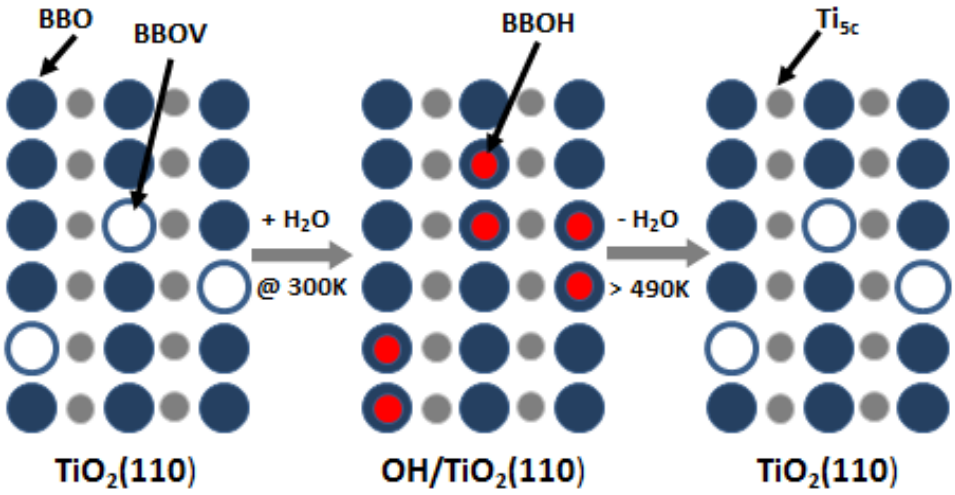

Figure 1.5: Schematic diagram of dissociative adsorption of H_2O on BBOV sites and recombination of two BBOHs forming H_2O and a BBOV.

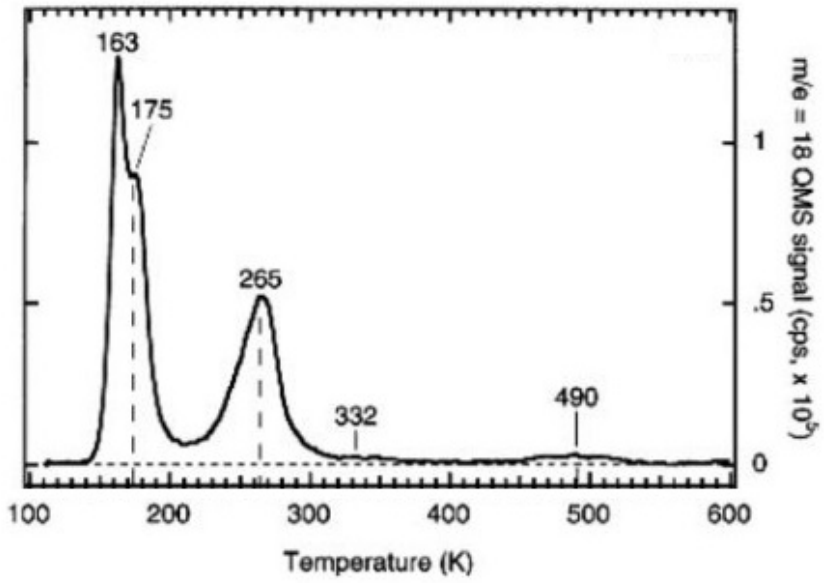

Figure 1.6: TPD spectra from a multilayer water adsorbed on TiO_2(110) at 110-118 K (heating rate 2 K s^{-1}). Figure is partially reproduced from Reference[18].

1.2.2 Hydrogen on TiO_2(110)

Hydrogen is directly related to energy issues and it is also one of the most common species in surface science research. Unlike H_2O on TiO_2(110), most of the behavior of molecular and atomic hydrogen on TiO_2(110) is still vague. H_2 has a low sticking coefficient for TiO_2(110)[9, 30]. On the contrary, atomic hydrogen can stick to TiO_2(110) at room temperature[30]. However, where adsorbed H atoms are located is still blurred. Unterberger et al. indicated that TiO_2(110) exposure to atomic H at 140 K produced hydroxyls[31]. Experimental and theoretical studies of a (1×1) adlayer of atomic H on TiO_2(110) by Wöll et al. indicated that H migrates into the bulk upon heating, in good

agreement with the previous results of an IR study by Yates et al.[32], instead of desorbing as H_2O or H_2[33]. Nonetheless, Du et al. found H atoms produced by trimethyl acetic acid dissociative adsorption and subsequent photolysis are bound to BBO, and above 300 K, the BBOHs will recombine to form H_2O, excluding the H diffusion into the bulk[34]. In addition, Iwasawa et al. showed that atomic H on TiO_2(110) exists in two forms, Ti-H and Ti-OH, by their STM and ESD studies[35].

1.3 Previous Electron Stimulated Desorption Study of TiO_2(110)

Electron Stimulated Desorption (ESD) is a high-sensitivity tool to study TiO_2(110), though the reference of literatures that contain both ESD and TiO_2(110) is limited. The purposed of early researches of ESD on TiO_2(110) were to study some basic issues, such as identification of ions[36-39], thermal stability of ESD of O^+ ions[40], influence of surface reduction on adsorption of gases[41-42], metallic surface layers[43-44], and orientation of adsorbed species[45]. From 2000, researches of ESD on TiO_2(110) were more focused on the behavior of adsorbed small molecules on TiO_2(110). Madey et al. found different ESD behavior of NH_3 preadsorbed on stoichiometric and oxygen deficient surfaces[46]. Kimmel et al. studied <3 monolayer (ML) water films on TiO_2(110) by ESD and found different products of desorption during irradiation[47], and they further found multilayer water films can weaken the excitations in TiO_2 and ESD of H from water on Ti_{5c}[48]. Their work of

water on TiO_2(110) includes not only ESD but also electron-stimulated reaction. Recently, ESD studies of O_2/TiO_2(110) showed efficient charge transfer from adsorbed oxygen species (O_t, from O_2 dissociated at Ti_{5c}) to the Ti(3d) level accounts for a high O^+ ESD yield from O_t compared to lattice oxygen[49]. Also, the band bending efficiency of charge transfer across TiO_2(110) were investigated by ESD of O_2/TiO_2(110) and adding electron donor/accepter molecules to the surface[50]. Moreover, the kinetics of surface and bulk electron-hole pair recombination on TiO_2(110) was measured by using ESD of O_2/TiO_2(110) as a probe[51].

1.4 Electron Stimulated Desorption Mechanisms

Besides TiO_2(110), ESD has been widely used to study various metal and semiconductor surfaces, including Pt(111), Ni(110), Ni(111) and Si(110)[52]. Many mechanisms were proposed for ESD from surfaces, and they are reviewed in Reference[52-53]. In this section, two models will be mainly discussed, which are more closely related to the study of TiO_2(110) surface in this thesis.

1.4.1 Menzel-Gomer-Redhead (MGR) Mechanism

The Menzel-Gomer-Redhead model was proposed independently by Menzel and Gomer in Chicago[54] and Redhead in Ottawa in 1964[55]. The acronym MGR is applied to this model. It is one of the earliest and general models to explain ESD from surfaces. It

incorporates adiabatic approximations and a semiclassical description of possible excitations to a surface-adsorbate system (Figure 1.7). It is a two-step mechanism. The first step is the ionization or excitation of an adsorbed atom or molecule by electron impact, which is similar to the Frank-Condon transition. An electron can be removed from one of the stable levels of an adsorbed species, resulting in a charged or excited adsorbate, whose interaction energy curve with the substrate may be very different from that of the neutral adsorbate. The second step is that the charged or excited adsorbate can either escape from the surface as an ion or excited neutral species (Figure 1.7a) or ground state neutral species (Figure 1.7b). In the first case, the system will relax by the excited adsorbate moving away from the surface, thus reducing the potential energy and imparting equivalent kinetic energy to the excited adsorbate. If no further processes intervene, the ion or excited neutral species will escape the surface into the vacuum with a kinetic energy range as shown in Figure 1.7a. The second case can be explained similarly in Figure 1.7b. The excited adsorbate is very close to the surface, so it has a finite probability of being reneutralized by an Auger or resonance neutralization process. The net result is that the excited adsorbate returns to the ground state but with some kinetic energy. If this kinetic energy is larger than the potential energy difference between that represented by the ground state curve at the point of de-excitation and the vacuum level, the adsorbate can escape from the surface as a neutral species.

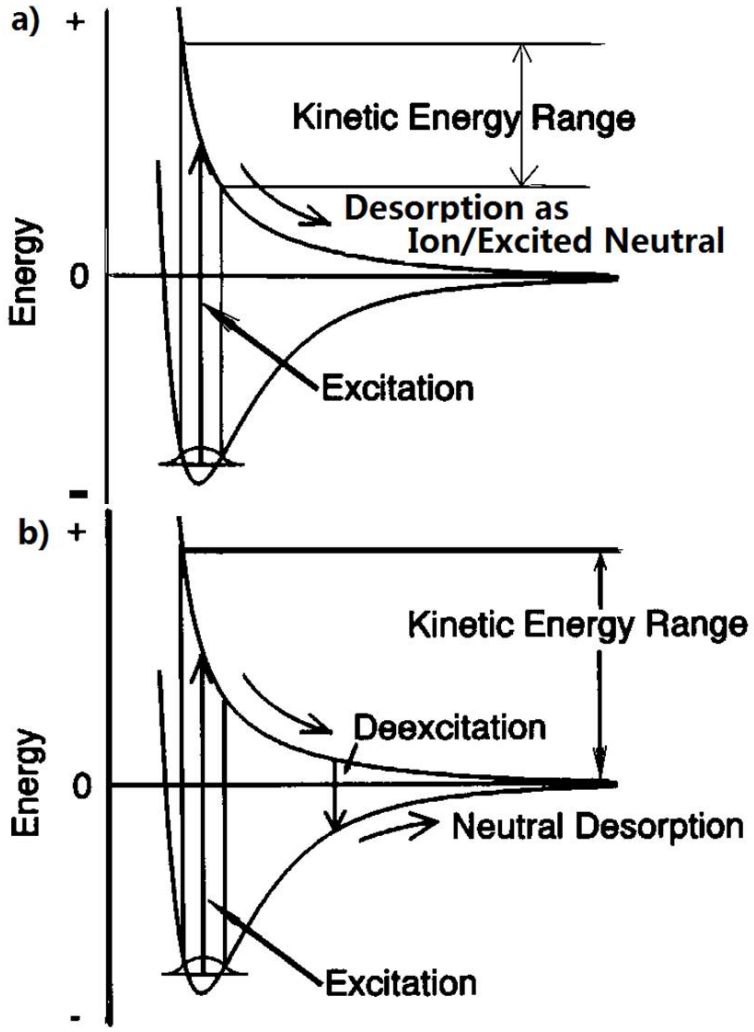

Figure 1.7: Schematic diagram showing the processes involved in the ESD of an adsorbate as (a) an ion or excited neutral species or (b) ground state neutral species, according to the MGR model.

1.4.2 Knotek-Feibelman (K-F) Mechanism

In 1978, Knotek and Feibelman (K-F)[56] proposed a model for O^+ desorption from TiO_2 and other highly ionic maximal valence oxides, such as V_2O_5 and WO_3 . This

mechanism is based on the observation that the threshold energy for O^+ ESD from TiO_2 corresponds to the excitation energy of Ti(3p) core level (34 eV). To rationalize the formation of an O^+ ion from an O^{2-} species, it was proposed that the Ti(3p) core hole is filled with electrons from O(2p) orbitals via an inter-atomic Auger process from a neighboring O^{2-}. It was also argued that since no electron exists at the Ti(3d) level in the Ti^{4+}, no intra-atomic Auger process from the Ti(3d) level to the Ti(3p) level will occur. If three electrons escape from the oxygen, the O^{2-} becomes O^+. This O^+ ion can then be ejected from the surface by Coulomb repulsion from the surrounding Ti^{4+} ions in the lattice.

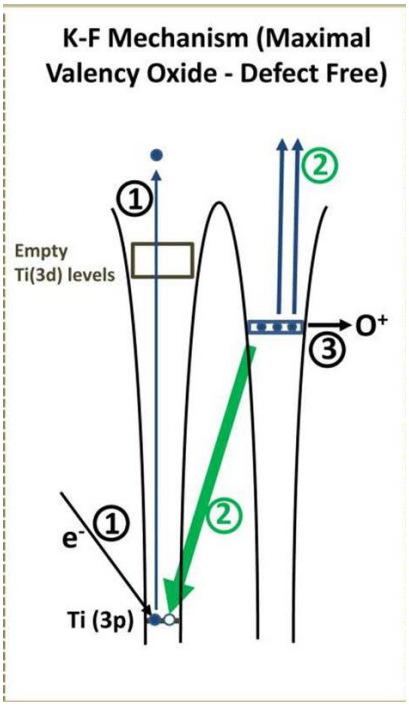

Figure 1.8: Schematic diagram of Knotek-Feibelman (K-F) mechanism for O^+ ESD from a TiO2 surface. Figure is reproduced from Reference[57].

CHAPTER TWO: Instrumentation and Sample Details

2.1 Ultra-high Vacuum Apparatus

The surface experiments presented in this thesis were conducted in a stainless steel ultrahigh vacuum (UHV) chamber equipped with several surface analysis techniques. This chamber operates at a base pressure of $< 3 \times 10^{-11}$ mbar, which is measured by an ionization gauge located in the lower portion of the chamber. The ultrahigh vacuum is kept by a turbomolecular pump (Leybold-Heraeus), an ion pump (Leybold-Heraeus) and a titanium sublimation pump (Leybold-Heraeus).

2.2 Instrumentation, Methods and Sample Details

The UHV system is equipped with the following surface analysis tools in the upper portion (Figure 2.1): (1) a combined time-of-flight electron-stimulated desorption ion angular distribution (TOF-ESDIAD), (2) a pulse counting low energy electron diffraction (LEED), a cylindrical-mirror-analyzer-Auger electron spectrometer (CMA-AES, Perkin-Elmer), (3) a differentially pumped and shielded and apertured quadrupole mass spectrometer (QMS, UTI 100C) for temperature programmed desorption (TPD) measurements and photon stimulated desorption (PSD) measurements, (4) a ultraviolet (UV) source (500 W Hg arc lamp, Oriel), whose light is conducted by fiber optics into the

vacuum, (5) an ion gun for Ar^+ sputter cleaning, and (6) a collimated and calibrated microcapillary array doser.

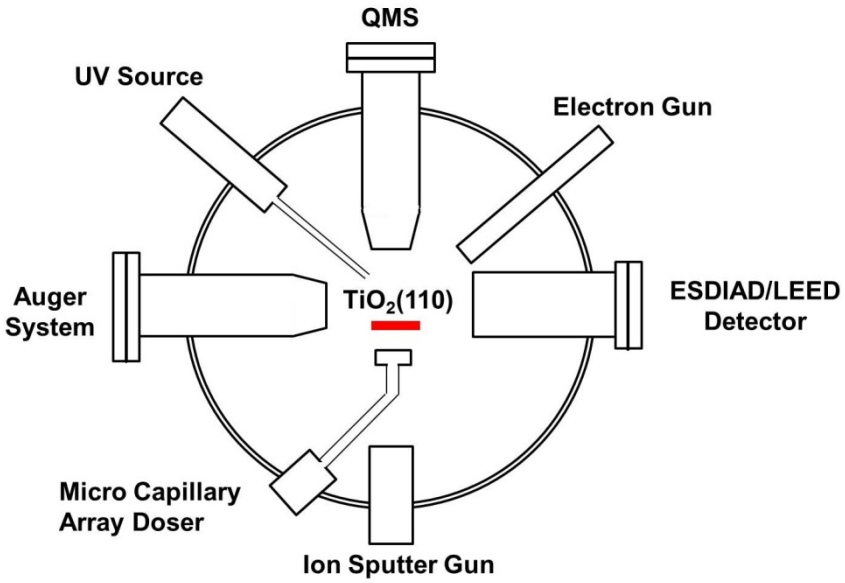

Figure 2.1: Top-down schematic diagram of the UHV chamber and surface science tools.

2.2.1 Time-of-flight Electron Stimulated Desorption Ion Angular Distribution

The diagram of ESDIAD is shown in Figure 2.2. The incident pulsed electron beam with frequency of 2-40 kHz and width of 50 ns, is obtained by an electron gun of 180 eV and a square pulse generator (Avtech, AVR-E2-PS). Atoms or molecules on the surface can be excited by the electron beam and be ejected from the surface as ions (usually positive ions) or neutral species. We apply a positive voltage (+30 V) on the crystal to suppress the secondary electron emission. The first two hemispherical grids (G_1 and G_2) are at ground

potential, and the G_4 is biased by -1.2 kV, so that the emitted positive ions are guided to accelerate toward the microchannel plates (MCPs). G_3 is biased by +10 V to avoid low energy ions hitting the MCPs to reduce the noise. When an ion hits the first MCP, it produces an electron cascade. The electrons then hit the second MCP and produce more electron cascades. The electrons generated from the second MCP hit the resistive anode (RA), where signals are generated and imported into an analog position computer (Model 2401, Surface Science Laboratory), which subsequently calculates the coordinates (x, y) of the position of electron impact. The arriving time of ions are subsequently analyzed by a pico-timing discriminator (Ortec) and a time amplitude converter (Ortec). The time-of-flight (t) of a detected ion is determined by the difference between the electron pulse and the arriving time. The x, y and t information is digitized by two Nuclear Data ADCs (ND 581) and a Fast Comtech ADC (Model 7070) and then transported to a computer, where the MPANT software (FAST ComTec) is used for data analysis and visualization. The major characteristics of this software used in this thesis are the time-of-flight spectra of ions and ion angular distribution patterns of peaks.

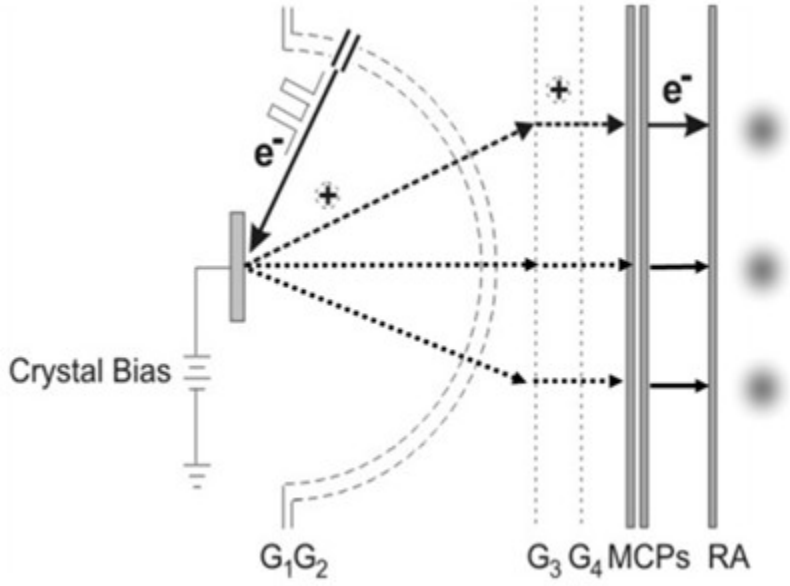

Figure 2.1: Diagram of ESDIAD.

2.2.2 Low Energy Electron Diffraction

In this thesis, low energy electron diffraction (LEED) is used as an auxiliary tool to assure that the single crystal TiO_2(110) is in a well-ordered (1×1) surface structure. The mechanism of LEED is described as follows: In LEED, monochromatic incident electrons (20-1000eV) which are elastically scattered back from a surface are analyzed; if the surface array is order, an ordered LEED pattern is achieved. The LEED mode can be fulfilled by changing the grid polarity and electron energies, and using continuous electron beams instead of pulsed electron beams, based on the settings of TOF-ESDIAD. Thus, LEED

patterns are obtained from the MPANT software. Figure 2.3 shows a clear LEED pattern of our sample. The value of b/a (2.16) is close to 0.649/0.295 (2.20)[9], indicating that the surface is (1×1).

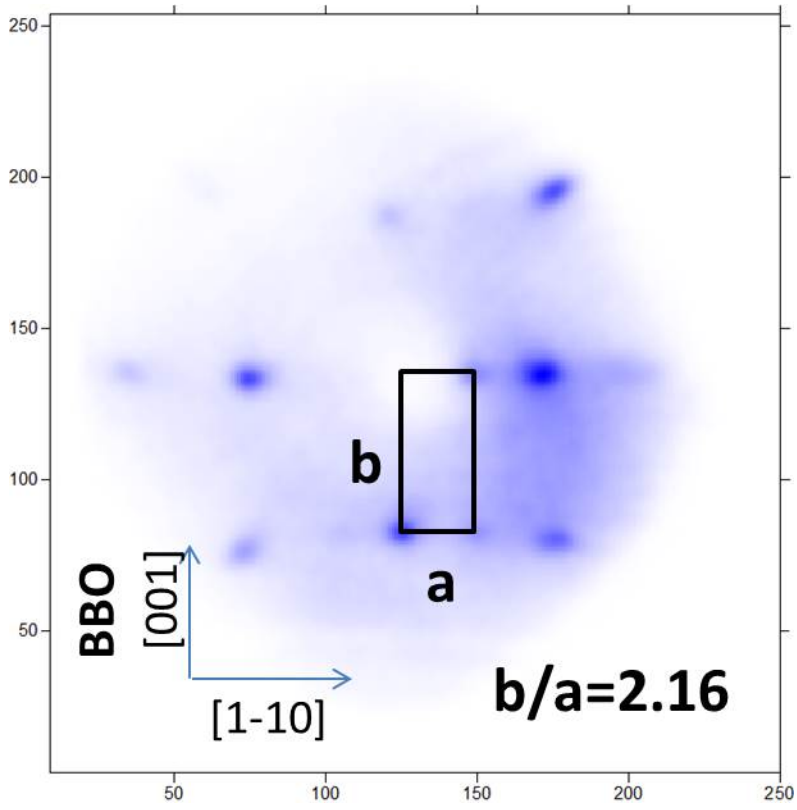

Figure 2.3: LEED pattern of TiO_2(110) used in this thesis showing its (1×1) order.

2.2.3 Auger Electron Spectroscopy

Auger electron spectroscopy (AES) is used as a supplementary tool to check the cleanliness of the TiO_2(110) surface, usually after the sample is exposed in air pressure and the UHV condition is rebuilt. Figure 2.4 illustrates the Auger effect. An incident high

energy electron knocks out a core electron and leaves a hole. The hole will be filled by an electron transition from an upper level. The energy released in this transition is removed as a photon (X-ray fluorescence) or by a third electron from upper levels: Auger electrons will then escape into the vacuum with discrete kinetic energies. The Auger electrons are element specific (not applied to H and He) and thus can be used to determine the chemical composition of the surface.

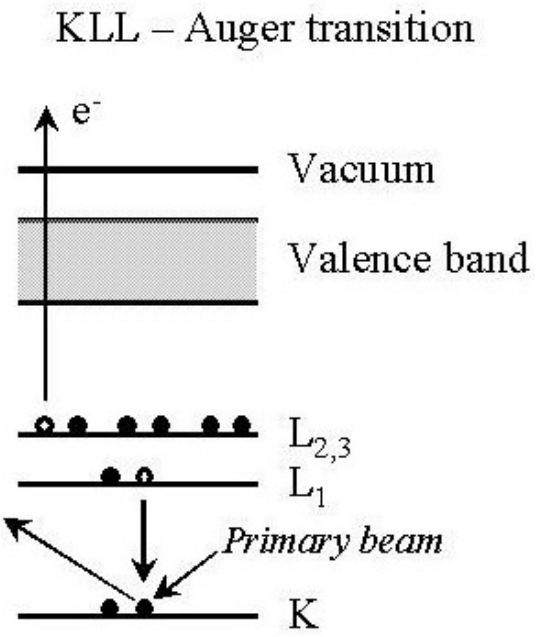

Figure 2.4: Schematic diagram of Auger process

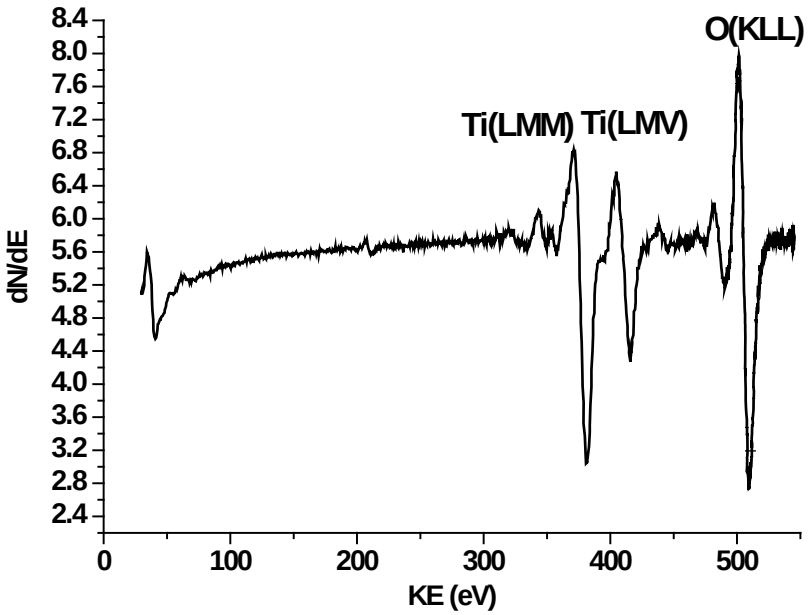

Figure 2.5: Auger electron spectrum of sputter-annealed TiO_2(110).

2.2.4 Quadrupole Mass Spectrometer

In our experiments, quadrupole mass spectrometer is mainly used for residual gas analysis, checking the impurity of gases, and monitoring the desorbed species in TPD and PSD experiments. (Figure 2.6)

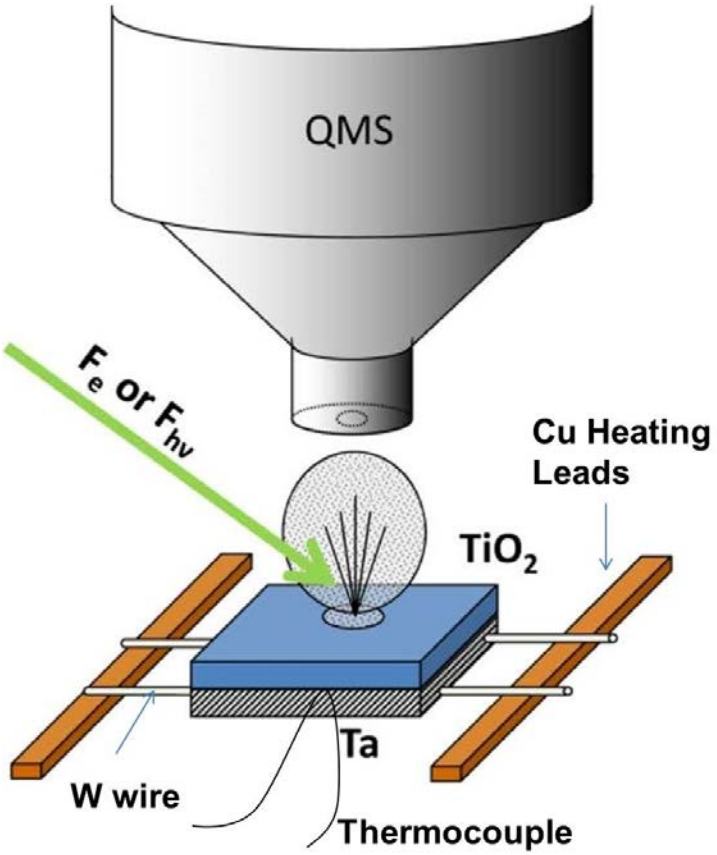

Figure 2.6: Diagram of TPD-QMS or PSD-QMS, and TiO_2(110) mount. The incident electron flux (F_e) is 10^{10}-10^{14} electrons cm^{-2} s^{-1}, and the incident photon flux (F_{hv}) is ~10^{14} photons cm^{-2} s^{-1}.

2.2.5 Temperature Programmed Desorption

In temperature programmed desorption, a constant temperature ramp (dT/dt) is applied to the sample and the QMS is used to monitor the species desorbed from the surface. Both the control of temperature and monitor of QMS signals are operated through the software LabVIEW.

2.2.6 Photon Stimulated Desorption

In photon stimulated desorption, the UV light is applied to the sample and QMS is used to monitor the species desorbed from the surface. The UV source (500 W Hg arc lamp, Oriel) generates photons of energies ranging from near-IR to UV (Figure 2.7). A 10-cm long IR filter filled with water is used to screen the portion of IR. Besides, longpass filters (Andover, Edmund) and bandpass filters (Newport, Andover) are used to achieve UV photons of desired energies. The filtered UV light is conducted by the fiber optics into the vacuum. The fiber material used in both feedthrough and cable is pure 600μm silica core with a doped silica cladding.

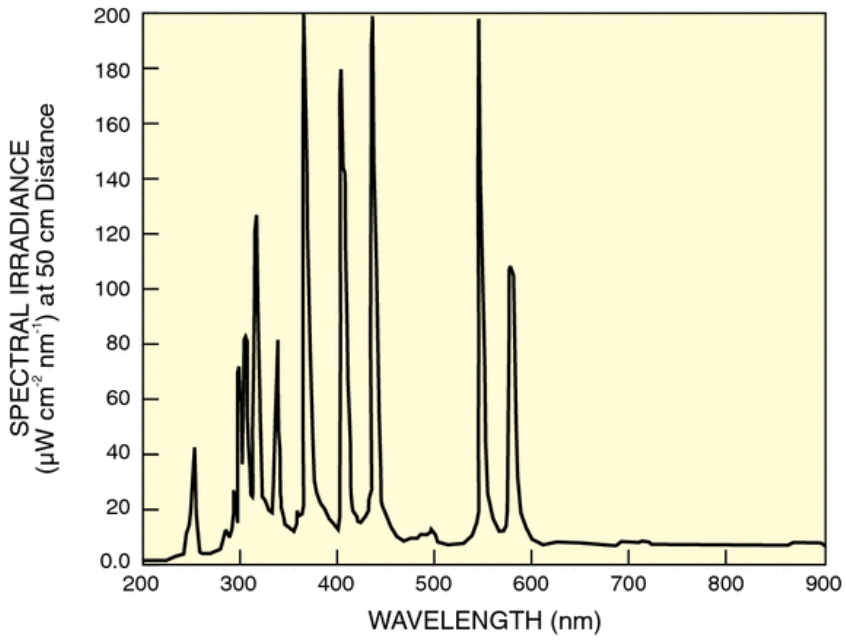

Figure 2.7: Spectrum of typical output of a 500 W Hg arc lamp[58].

2.3 TiO_2 Sample Mounting, Cleaning and Preparation

The polished rutile TiO_2(110) single crystal (Princeton Scientific, 7×7×1 mm^3) is cemented (using AREMCO 571 cement) onto a Ta support plate to facilitate thermal contact (Figure 2.6). No part of the Ta plate is exposed in the forward direction, and only the crystal is seen in measurements and microcapillary array dosing[59]. Two tungsten wires are spot-welded onto the back of the Ta plate for resistive heating. The temperature of the crystal is measured and electronically controlled by a type-K thermocouple (chromel-alumel) cemented (AREMCO 571 cement) to the back center of the crystal through a hole in the Ta plate. The crystal is cleaned by Ar^+ sputtering (1000 eV, 45 min) followed by annealing (950 K, 10 min) before experiments.

2.4 Gas Handling and Dosing

In this thesis, two methods are employed to expose gas to the surface or into the chamber: background dosing and microcapillary array dosing. Background dosing is used commonly in checking the impurity of gases. Besides, in Chapter 4, dosing atomic H onto the surface is achieved by pyrolysis of H_2 backfilled into the vacuum. In most other cases, gases are dosed to the surface through a microcapillary beam doser. This doser is calibrated by $^{16}O_2$ and the flux is $F_{O_2}=1.67\times10^{12}$ molecules $torr^{-1}$ s^{-1} (measurement made by Zhen Zhang). The flux of another gas A is calculated by $F_A=F_{O_2}(M_{O_2}/M_A)^{1/2}$, where M = gas

molecular weight.

CHAPTER THREE: Defect-Electron Spreading on the TiO_2(110) Semiconductor Surface by Water Adsorption[57]

3.1 Abstract

The dissociative adsorption of water at oxygen-vacancy defect sites on the TiO_2(110) surface spatially redistributes the defect electron density originally present at subsurface sites near the defect sites. This redistribution of defect-electrons makes them more accessible to Ti^{4+} ions surrounding the defects. The redistribution of electron density decreases the O^+ desorption yield from surface lattice O^{2-} ions in TiO_2, as excited by electron stimulated desorption (ESD). A model in which OH formation on defect sites redistributes defect electrons to neighboring Ti^{4+} sites is proposed. This switches off the Knotek-Feibelman mechanism for ESD of O^+ ions from lattice sites. Conversely, enhanced O^+ reneutralization could also be induced by redistribution of defect electrons. The redistribution of surface electrons by adsorption is further verified by the use of donor and acceptor molecules which add or remove electron density.

3.2 Introduction

The TiO_2(110) surface is a widely-used model oxide surface for thermally-activated

catalysis as well as for photocatalysis and photovoltaic processes induced by UV light[8-9, 60-61]. Water has been thoroughly investigated as an adsorbate on TiO_2(110) and the practical conversion of water to hydrogen and oxygen on TiO_2 surfaces using solar energy is a promising goal, building on the early pioneering work of Honda and Fujishima[1]. Bridge-bonded oxygen vacancy (BBOV) sites on the surface, formally associated with two defect electrons in their vicinity, play an important role in determining the surface reactivity of TiO_2(110)[9, 62]. Water molecules dissociate at BBOV sites producing an –OH group (called BBOH) at the vacancy and also a second –OH group at a nearby BBO site (see inset in Figure 3.1)[14, 22, 63]. Heating to ~ 490 K causes two BBOH groups to recombine, producing H_2O(g) and regenerating a BBOV site[17].

An electronic state with energy ~0.8 eV below the Fermi level on TiO_2(110), which participates in the chemical bonding of adsorbed molecules, is fully or partially associated with the defect electrons on BBOV sites[64-67]. This defect electronic state is hardly influenced in energy or intensity by water dissociation on the defect sites, as demonstrated by both photoemission spectroscopy[64, 68] and electron energy loss spectroscopy[15]. Furthermore no additional electronic states in the bandgap region are produced by BBOH adsorption on defect sites. The filling of the BBOV sites by BBOH formation does not influence the TiO_2 surface reactivity toward O_2[69]. The above observations raise an interesting question about the spatial distribution of the defect-electrons associated with

the defect sites before/after the dissociative adsorption of H_2O at these sites. This question has been explored by experiments and by theoretical calculations [70-72]. The presence of Ti^{3+} on the defective TiO_2 surface as seen by experimental measurements [15, 68, 73-75] indicates that the defect-electrons are localized on nearby Ti atoms, formally reducing Ti^{4+} to Ti^{3+}. Using the resonant photoelectron diffraction (PED) method, Krüger *et al.* [65, 74] found that most defect charge is distributed on the subsurface Ti atoms, especially on the second layer Ti atoms. Recent theoretical results [76-79] also proposed that the defect-electron on defective TiO_2 surface is localized on one Ti atom and induces a local lattice distortion forming a polaron. The mobile polarons with low activation energy for motion in the surface and subsurface region make the defect-electrons appear to be delocalized near the surface. [79-80] The influence of the dissociative adsorption of H_2O on defect sites on the spatial distribution of defect-electrons is still an open question. Combining STM and DFT calculations, Minato *et al.* [81] found that the defect-electrons at both BBOV and BBOH sites appear to be delocalized along the surface. Di Valentine *et al.* [72, 82] found that the defect site and the BBOH site both involve a spatially-localized electronic state; in contrast, Liu *et al.*[19] theoretically observed delocalization of the electronic state when BBOH was produced at the BBOV defect sites.

Our experiment to be described below suggests that the defect electrons are ***spread out*** spatially by OH formation near BBOV sites. This could be due to actual delocalization

of electron wavefunctions or their redistribution to other Ti sites. From the experiment it is impossible to separate these two concepts relating to spreading of defect electrons by H_2O dissociative adsorption.

3.3 Experimental Section

The experiment was carried out in a stainless steel UHV chamber (base pressure below 3×10^{-11} mbar) equipped with a combined time-of-flight electron stimulated desorption ion angular distribution (TOF-ESDIAD) and pulse counting low energy electron diffraction (LEED) apparatus, a cylindrical-mirror-analyzer-Auger electron spectrometer (CMA-AES), and an apertured quadrupole mass spectrometer (QMS). A TiO_2(110)-(1×1) crystal (Princeton Scientific, 7×7×1 mm^3) with BBOV density of 10% BBO sites on the surface was prepared by cycles of Ar^+ sputtering and annealing in UHV at 950 K. The cleanliness and surface structure of the TiO_2(110)-(1×1) surface was confirmed by AES and LEED, respectively. A partially-hydroxylated TiO_2(110) surface was then prepared by exposing to water vapor at 300 K from a calibrated and collimated molecular beam source. The complete dissociation of water on BBOV sites occurs and intact water molecules are not present on the surface at the low coverage and adsorption temperature employed. The ESD experiments on the TiO_2(110) surface employed pulsed 180 eV electrons at 40 kHz with 75 ns width, and the produced positive ions are separated by their time-of-flight caused by the ion mass difference [83]. A +30 V or +40 V bias was applied to

the sample during the ESDIAD measurements of the angular distribution of desorbing ions. Adsorption of gases, such as $^{15}N^{18}O$, $^{18}O_2$, ND_3, and C_5D_5N from the calibrated beam was also carried out. The temperature-programmed desorption (TPD) of H_2O molecules used a heating rate of 2 K s^{-1} and desorbing products were detected by the line-of-sight QMS.

3.4 Results and Discussion

Figure 3.1 shows the time-of-flight distribution of H^+ and O^+ ions produced by ESD on the TiO_2(110) surface. On the clean TiO_2(110) surface containing 10% BBOV sites (curve a), O^+ ions originating from BBO surface lattice O^{2-} sites were observed at a flight time of 2.2 μs. A trace amount of H^+ from BBOH due to the dissociation of residual H_2O (in UHV) on the BBOV sites was also observed at a flight time of 0.5 μs. After exposing the TiO_2(110) surface to 7.2×10^{13} H_2O molecules cm^{-2} at 300 K, water molecules were dissociated at the surface, filling the BBOV sites, and each H_2O molecule formed two BBOH species (upper inset in Figure 3.1). On the hydroxylated TiO_2(110) surface (curve b), a huge yield of H^+ from BBOH species was observed. Most notably however, the O^+ signal decreased significantly upon adding a small coverage of H_2O undergoing dissociative adsorption. The similarity of TOF distributions and ESDIAD patterns (right-hand insets) of O^+ in (a) and (b) indicates that the presence of BBOH on the TiO_2(110) surface does not change the energy and spatial direction of O^+ desorption by ESD, consistent with these ions originating from lattice surface O^{2-} species. Statistically, at

the low BBOH coverages employed here, the O^+ species mainly originate from O^{2-} lattice sites at a large distance from the BBOH species.

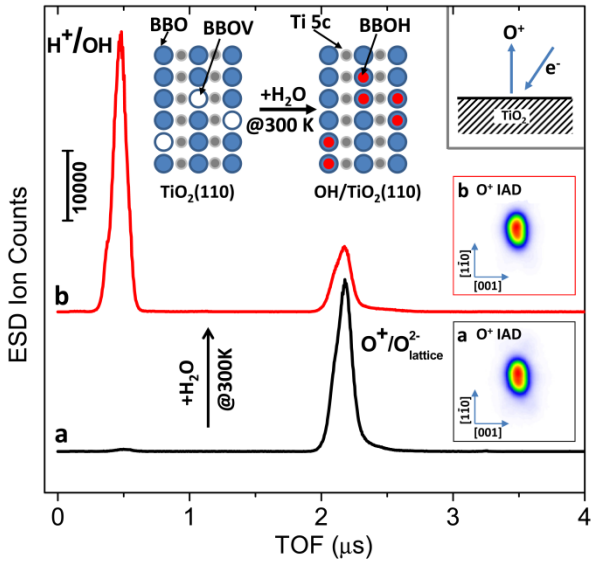

Figure 3.1: Time-of-flight distribution of ESD-produced H^+ and O^+ from TiO_2(110) surfaces containing either BBOV (curve a) or BBOH (curve b) surface sites. The production of a small coverage of BBOH species on the TiO_2 surface significantly decreases the O^+ ESD yield. The ESDIAD patterns of O^+ indicate that the ion angular distribution (IAD) of O^+ ions from the lattice sites is unchanged for dissociative H_2O adsorption.

The coverage of BBOH sites on the TiO_2(110) surface following H_2O adsorption can be quantitatively determined by measuring the yield of recombinative desorption of H_2O from BBOH association at higher temperature: $2BBOH \rightarrow BBO + BBOV + H_2O$ [17]. This measurement then permits the fraction of BBOV sites before H_2O adsorption to be determined. Using this method, the measured coverage of BBOV sites is about 0.1 ML after clean crystal preparation. The measurements are shown in the inset of Figure 3.2

where the TPD process from 1.5 ML of H_2O is shown. This total H_2O desorption consists of a fraction of second-layer H_2O associated with BBO sites, a fraction of first-layer H_2O associated with Ti_{5c} sites, and a fraction of H_2O made by the BBOH recombination process and observed at the highest temperature [23, 84]. The derived BBO coverage for the clean surface is therefore about 0.9 ML, consistent with the work of many others[23, 67, 84]. As H_2O is adsorbed, as shown in the main part of Figure 3.2, the BBO fractional coverage is found to decrease from 0.9 to 0.8 ML as shown by the blue curve as BBOH species are produced by water adsorption. The inset to Figure 3.2 shows that the BBOH coverage reaches a maximum after an exposure to ~5×10^{13} H_2O molecules/cm^2 at 300 K, which produces about 0.2 ML of BBOH species, equivalent to the consumption of about 0.1 ML of BBOV sites. Our central finding is that the effect of the addition of an OH species influences about 5x as many neighbor O^{2-} lattice sites by shutting down O^+ formation in ESD. The factor of 5 magnification in the fractional loss of O^+ ESD signal compared to the production of BBOH species (~0.1 ML) argues persuasively that a simple geometrical site blocking model is inappropriate and that instead a *longer-range* ESD quenching effect across the TiO_2 surface, originating from the formation of BBOH species, is being observed. This long range effect is postulated to be due to the redistribution of defect-site electrons across the surface when BBOH species are formed at BBOV sites, which will be discussed later.

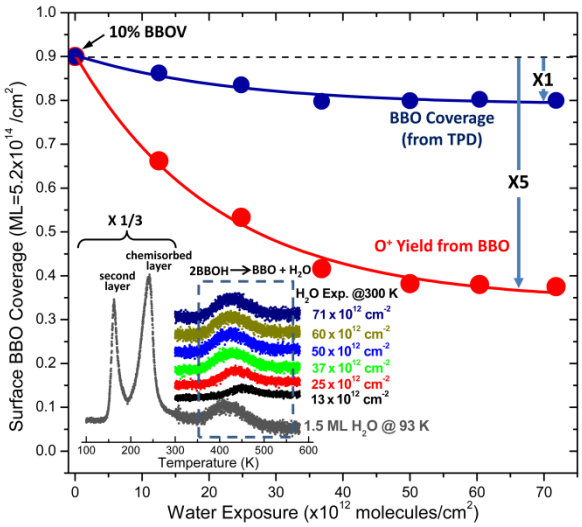

Figure 3.2: The influence of water exposure on the O^+ ESD yields. Inset shows the TPD spectra of H_2O on the TiO_2(110) surface showing that $2BBOH \rightarrow BBO + BBOV + H_2O$ occurs near 420 K. The BBO coverage (blue dots) on the water-exposed TiO_2(110) surface at 300 K is calculated by the comparison of the H_2O recombinative desorption yield to the H_2O yield from 1.5 ML H_2O at 93K. The red dots indicate the O^+ ESD yield from BBO related to the O^+ yield from the clean TiO_2(110) surface, both of which are normalized to the initial BBO concentration (0.9). A negative temperature measurement error of ~70 K near 400 K exists in the TPD spectra.

To further test the idea that the spreading of electron density at the TiO_2 surface significantly influences the production of O^+ ions by ESD, we employed the adsorption of both electron-acceptor molecules and electron-donor molecules to remove or add electron density to the surface as shown in Figure 3.3. Electron acceptor molecules, $^{15}N^{18}O$ and $^{18}O_2$ were employed to trap the spread-out defect-electrons. Oxygen isotopic labeling of the electron acceptor molecules was used to eliminate interference with measurements of the $^{16}O^+$ ESD yield from the TiO_2 lattice. The transfer of electrons from hydroxylated

TiO_2(110) to adsorbed NO has been shown to occur using STM and XPS measurements as well as by DFT calculations [21]. The transfer of electrons from the hydroxylated TiO_2(110) to adsorbed O_2 has also been measured by EELS [15]. For both acceptor molecules used here, it was found that transfer of charge from the surface strongly increases the yield of O^+, as expected for the partial removal of the spread-out defect-electrons. In contrast, the electron-donor molecules, ND_3 and C_5H_5N, cause a decrease in the O^+ ion ESD yield from the TiO_2 lattice as shown in the bottom of Figure 3.3. This is caused by the enhancement of electron density on the surfaces by the donor molecules.

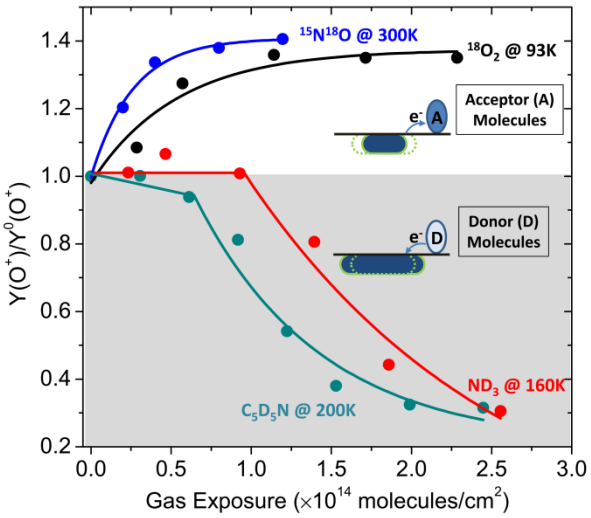

Figure 3.3: Manipulation of electron density at the hydroxylated TiO_2 surface. The adsorption of electron acceptor molecules ($^{15}N^{18}O$, $^{18}O_2$) enhances the O^+ ESD yields due to the electron transfer from TiO_2 to the acceptor molecule causing a loss of delocalized electron density across the TiO_2 surface. On the other hand, the presence of electron donor molecules (ND_3, C_5D_5N) decreases the O^+ ESD yields due to the electron transfer from the donor molecule to TiO_2 causing an enhancement of delocalized electron density. The inactive zone at low coverages of the donor molecules is due to their initial adsorption on BBOH groups by hydrogen bonding [85-86].

The spatial distribution of defect electrons associated with BBOV defect sites on the TiO_2(110) surface is schematically indicated in Figure 3.4a. These electrons, while associated with the O^{2-} vacancy, may be distributed amongst Ti^{4+} ions at a depth of one or two lattice distances under the surface.[65, 74, 76-79] After dissociative adsorption of water, the defect-electrons redistribute along the surface. This is possibly related to the lattice relaxation by the filling of BBOV sites with BBOH species. The electron-spreading effect is schematically indicated by the small red hatched regions at surface-Ti sites. Using DFT

calculations, Liu *et al.* [19] found that the presence of BBOH on TiO_2(110) surface causes the spread of defect-related electrons along the [001] direction, in agreement with this general idea.

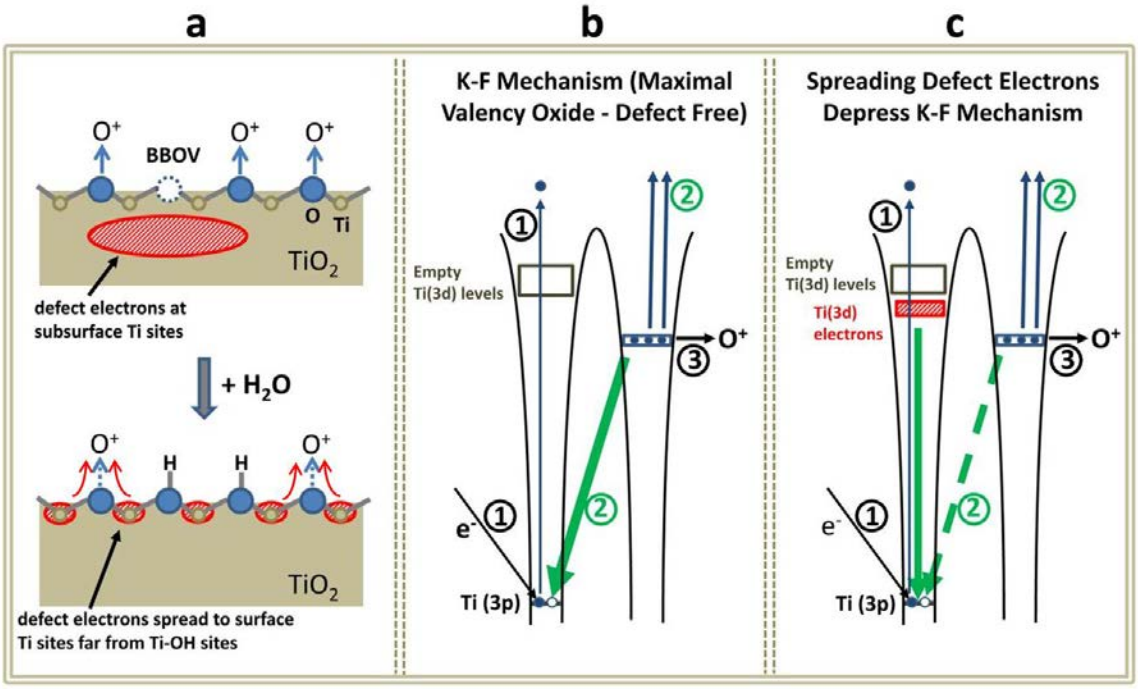

Figure 3.4: The influence of Ti(3d) electron distribution on the O^+ ESD yields. (a). The schematic distributions of defect electrons on TiO_2(110) surface with BBOV sites (upper part) and BBOH sites (lower part). (b). Schematic diagram of Knotek-Feibelman (K-F) mechanism for O^+ ESD from a TiO_2 surface triggered by the production of a hole in the Ti(3p) level; (c). The influence of defect Ti(3d) electron distribution on the K-F mechanism, showing that a spread-out electron distribution influencing multiple Ti(3p) sites enhances the transitions from the Ti(3d) electrons to Ti(3p) hole sites, depressing the K-F O^+-yield in processes 2 and 3.

The depression of the O^+ ion yield in ESD on the hydroxylated TiO_2(110) surface by the redistribution of defect-electrons along the surface may occur via two mechanisms: (i)

The redistributed electrons can depress the initial formation of O^+ at the initial stage (initial state ionization effect); (ii) The redistributed electrons can more effectively reneutralize the O^+ ions formed by ESD (final state reneutralization effect).

(i) *Initial State Ionization Effect:* The generation of O^+ ions by ESD on TiO_2 has been proposed to occur by a well-known process - the Knotek-Feibelman (K-F) process - as shown in Figure 3.4b [56]. According to the K-F model, the maximal valency defect-free oxide (stoichiometric TiO_2) containing only Ti^{4+} ions in the surface and throughout the bulk, contains no electron density in the empty Ti(3d) valence band. When an incident electron (with a threshold energy of ~34 eV) [56, 87] excites the semiconductor TiO_2 by process 1, the ejection of an electron occurs from the Ti(3p) core level. Since there is no Ti electron density in the empty valence band, an interatomic Auger transition ─ process 2, heavy solid green arrow involving O(2p) electrons ─ takes place to fill the Ti(3p) hole. To conserve energy, two additional O(2p) electrons are also ejected in process 2, leaving an O^+ lattice ion where an O^{2-} surface lattice ion was originally present. A Coulomb explosion, ejecting the O^+ ion from the lattice containing repulsive Ti^{4+} ions is the result, and lattice O^+ is observed to desorb in ESD ─ process 3. In a traditional Auger transition, valence electrons of the Ti atom would fall into the Ti(3p) hole (intra-atomic Auger transition) but in maximal valency oxides this is impossible, and the less probable interatomic Auger transition occurs. Therefore, the O^+ ESD yield by the K-F process should vary inversely

with the occupancy of valence orbitals on the Ti^{4+} ions in the surface. Oxygen-vacancy (BBOV) defect sites, produce defect electron density at Ti^{4+} sites which participate in the downward Auger transition, shutting down the K-F mechanism and reducing the O^+-ESD yield. We postulate that the formation of BBOH species at BBOV sites causes the lateral redistribution of defect-electrons, causing the interatomic Auger transition to occur over a large region on the TiO_2 surface extending beyond the BBOH site, thereby further reducing the ESD yield of O^+ ions by the K-F mechanism.

The BBOH-induced spreading of electrons to neighbor Ti^{4+} sites enhances the overall probability of transition from the Ti(3d) electrons to the Ti(3p) holes, thereby short circuiting the K-F interatomic Auger process. This is shown in Figure 3.4c where the distribution of the defect electrons to multiple Ti(3d) sites is schematically represented by the cross-hatched regions. The suppression of the interatomic Auger process (short green dashes), caused by increased defect electron spreading along the surface, is accompanied by a decrease in O^+ yield by ESD over a wide area, as the K-F mechanism is shut down extensively. The formation of one BBOH site is responsible for suppression of the K-F mechanism at ~5 neighbor sites.

As a comparison, the H^+ ESD yields with the water exposure have also been investigated (Figure 3.5). The H^+ ESD yield scales proportionally to the BBOH coverage. This is reasonable because the H^+ ESD has a threshold energy at the O(2s) ionization not

the Ti(3p) ionization energy,[87] which means the redistribution of Ti(3d) electrons cannot influence the H^+ yields through the K-F mechanism.

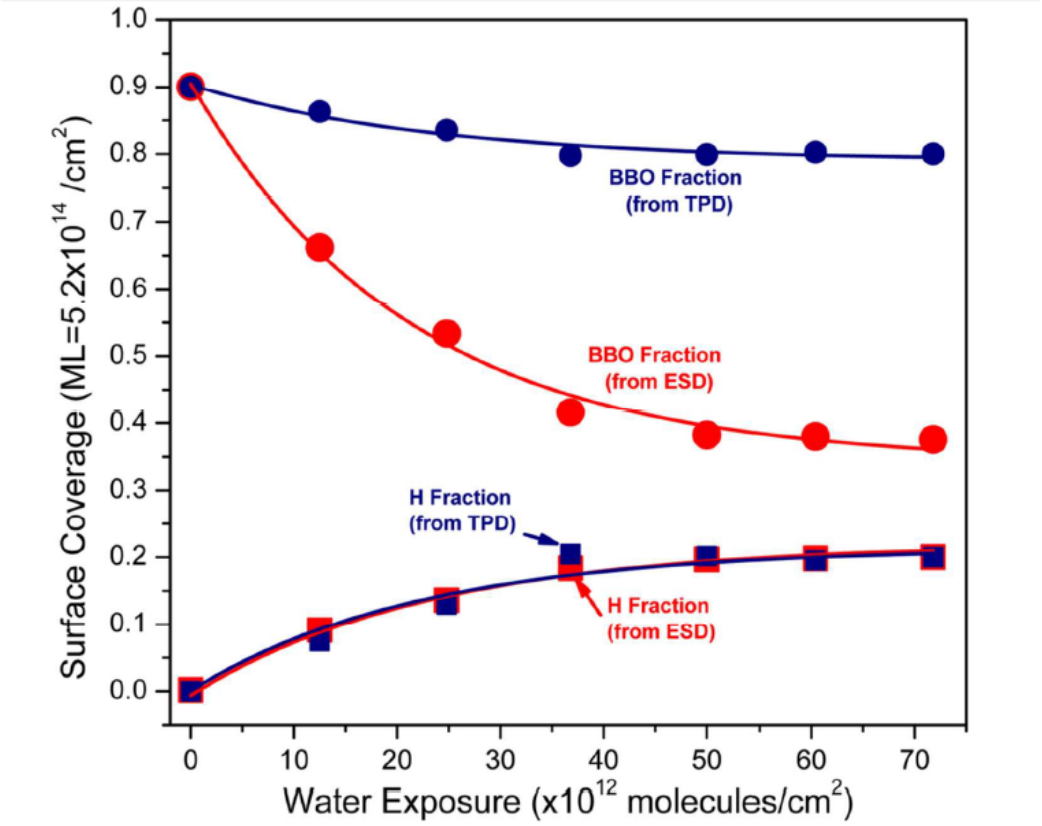

Figure 3.5: The BBO(blue dots) and BBOH (blue squares) show the coverages on the water-exposed TiO_2(110) surface at 300 K calculated from the magnitude of the H_2O recombinative TPD peaks. The red dots (squares) indicate the O^+ (H^+) ESD yield, which are normalized to the initial (final) BBO (BBOH) concentration. It is clearly seen that the fractional decrease in the O^+ yield far exceeds the fractional decrease in BBO coverage during H_2O adsorption.

It should be mentioned that the assumption of completely empty Ti(3d) orbitals in stoichiometric TiO_2 in the K-F mechanism is not strictly correct due to some degree of

covalency of Ti(3d) and O(2p) orbitals.[9, 88] Based on electron-ion coincidence spectroscopy measurements, Tanaka *et al.* [89] defined a new ionization mechanism in TiO_2 and proposed that instead of the interatomic Auger process in the K-F mechanism, electrons can directly transfer from the O(2p) orbitals to Ti(3d) orbitals due to the pulled-down Ti(3d) energy level by the Ti(3p) core hole leading to O^+ ejection. In this proposed mechanism, also, the enhancement of Ti(3d) electron availability can diminish the charge transfer between Ti(3d) and O(2p), decreasing O^+ production.

(ii) *Final State Reneutralization Effect:* The excited O^+ ions can also be reneutralized by the electrons transferred from the substrate or neighboring atoms, and thus the O^+ ESD yield decreases.[90-92] Within the framework of this model, the spreading of electron density by BBOH formation to neighbor sites would enhance O^+ neutralization.

It is not possible based on these experiments with BBOH groups or with donor and acceptor adsorbate molecules to discriminate between the initial and final state models proposed above.

3.5 Conclusions

In summary, we have shown that longer-range defect electron spreading may be chemically induced for electrons originally associated with oxygen vacancy defect sites on TiO_2(110). This longer range effect is postulated to be due to the redistribution of

defect-site electrons when BBOH species are formed at BBOV sites. This general finding is supported by the behavior of the O^+ yield in ESD, which is found to respond to electron donor/acceptor effects on the spread-out electrons. This finding may shed new light on the electronic behavior of oxide surfaces because of the dominant role of hydroxyl species in the surface chemistry of oxides of all types [80, 93]. For example, the longer-range interaction between BBOH and O_2 on the TiO_2(110) surface was investigated by DFT calculations, indicating that the spatial redistribution of defect-electrons may govern the O_2-supply pathways for CO catalytic oxidation on Au/TiO_2 catalyst surfaces [19].

CHAPTER FOUR: A New Form of Chemisorbed Atomic H on the TiO_2(110) Surface

4.1 Abstract

A new form of chemically-bound hydrogen, H/TiO_2, on the TiO_2(110) surface is produced by exposure to atomic H at 87 K. This chemisorbed hydrogen differs significantly in its physical and chemical properties from OH/TiO_2 species (BBOH) produced from H_2O dissociative adsorption. The H/TiO_2 species produces a normal beam of H^+ upon electron stimulated desorption whereas OH/TiO_2 species produce inclined H^+ ESD beams. By ~ 350 K, H/TiO_2 has desorbed thermally whereas OH/TiO_2 begins to desorb as H_2O only above ~350 K. Remarkably, H/TiO_2 exhibits an extremely large ESD cross section (7.1×10^{-14} cm^2), while the cross section for OH/TiO_2 is estimated to be ~10^{-20} cm^2. Moreover, H/TiO_2 is highly sensitive to UV photon desorption, while OH/TiO_2 is inactive to UV.

4.2 Introduction

Surface-bound hydrogen species on TiO_2 surfaces are involved in solar-driven reduction processes such as in the production of useful hydrogenated organic products from CO_2 and H_2O as well as H_2 from H_2O[1]. Such photochemical reduction processes

could become important in the capture, storage and transport of solar energy. Also in heterogeneous catalysis, atomic H spilled over from H_2 dissociation from metals supported on TiO_2[32, 94], and other oxides[95-96] or other metals[97-98], is important in surface reduction processes in the absence of light activation. Additionally, the absorption of H in TiO_2 significantly changes the TiO_2 geometric and electronic structure, increasing the solar light absorption efficiency and photocatalytic activity[99].

The rutile-TiO_2(110) surface is the prototype oxide surface, widely studied as a model photocatalytic material[8-9, 60-61] (band gap = 3.1 eV) as well as a model support for metallic catalyst particles[100-103]. It is a reducible oxide which may be partially reduced by heating in vacuum to 950 K and often exhibits up to ~10% oxygen-vacancy defects at its surface. In the bulk, while it can be made stoichiometric, it easily forms bulk oxygen vacancy defects[9] and associated Ti^{3+} interstitial species[64, 104] upon heating in vacuum. The non-stoichiometric character of TiO_2 causes it to be an n-type semiconductor. The rutile-TiO_2(110) surface is the thermodynamically most stable TiO_2 crystal surface.

As is common for all oxide surfaces, hydroxyl functional group bonding predominates. For TiO_2(110), Ti-OH groups can be made from water adsorption at oxygen vacancy defects producing 2 OH groups (BBOH) per adsorbed H_2O molecule[14, 22, 63].

On the other hand, the adsorption of atomic H on the TiO_2(110) surface has not been well studied but it has been reported that atomic H interacts with TiO_2(110) to

produce a Ti-OH surface species[33] in contrast to the work reported here. We demonstrate here the unique properties of the hydrogen surface species produced by atomic H adsorption which is bound to the TiO_2(110) surface in a new manner, differing from Ti-OH.

Electron bombardment of TiO_2(110) to cause electron stimulated desorption (ESD) has been used here to characterize the chemisorbed H species by the observation of the H^+ fragment product. H-bonding information is derived from the characterization of the H^+ kinetic energy, the measurement of the cross section for H^+ desorption in ESD, and the characterization of the H^+ angular distribution. We have used time-of-flight electron stimulated desorption (TOF-ESDIAD) and the measurement of total cross section for electron stimulated desorption along with the H^+ ion angular distributions by TOF-ESDIAD to characterize the new form of surface H (we tentatively term it as Ti-H), and to clearly distinguish it from Ti-OH species. In addition, UV induced photodesorption of H/TiO_2 has been observed and the cross section for photodesorption has been measured.

4.3 Experimental Section

This experiment was conducted in a stainless steel UHV chamber (base pressure below 5×10^{-11} mbar) equipped with a combined time-of-flight electron stimulated

desorption ion angular distribution (TOF-ESDIAD) and pulse counting low energy electron diffraction (LEED) apparatus, a cylindrical-mirror-analyzer-Auger electron spectrometer (CMA-AES), and an apertured quadrupole mass spectrometer (QMS) and a ultraviolet source. A TiO_2(110)-(1×1) crystal (Princeton Scientific, 7×7×1 mm^3) with BBOV density of ~6% BBO sites on the surface was prepared by cycles of Ar^+ sputtering and annealing in UHV at 950 K. The cleanliness and surface structure of the TiO_2(110)-(1×1) surface was confirmed by AES and LEED, respectively. A partially-hydroxylated TiO_2(110) surface (OH/TiO_2) was prepared by exposing to water vapor at 320 K from a calibrated and collimated molecular beam source. A hydrogenated TiO_2(110) surface (H/TiO_2) was prepared by exposing to atomic H at 87 K produced by pyrolysis of 1×10^{-7} mbar H_2 through background dosing on a ~1800 K tungsten filament. A PYRO Micro-Optical Pyrometer Set was used to measure the temperature of the tungsten filament. The ESD experiments on the TiO_2(110) surface employed pulsed 180 eV electrons at 2-40 kHz with 75 ns width, leading to different electron fluxes. The produced positive ions were separated by their time-of-flight caused by the ion mass difference [83]. A +30 V bias was applied to the crystal during the ESDIAD measurements.

4.4 Results and Discussion

Using 210 eV electrons and a pulse-counting ion angular distribution apparatus, it is found that both adsorbed OH (from partial monolayer (ML) H_2O adsorption) and H from

atomic H adsorption yield almost identical H^+ TOF distributions shown in Figure 4.1A. The 0.5 μs flight time, corrected for ion acceleration in the apparatus, corresponds to an H^+ kinetic energy = 9 ± 3 eV for ESD from both H/TiO_2 and OH/TiO_2 adsorbed species. While the ion energies are very similar, the ion angular distributions differ significantly as shown in Figure 4.1B and 4.1C. H/TiO_2 yields an almost circular normally-oriented H^+ angular distribution while OH/TiO_2 yields a highly elongated H^+ angular distribution. The elongation is in the $[1\bar{1}0]$ direction perpendicular to the rows of bridge-bonded oxygen (BBO) species as shown in the insert to Figure 4.1A. The normal H^+ ESDIAD pattern for H/TiO_2 indicates that the Ti-H bond is normally-oriented to the surface, while the elongated H^+ ESDIAD pattern for OH/TiO_2 indicates that the O-H bonds are inclined to the left or right in the $[1\bar{1}0]$ direction, or alternatively that high amplitude OH bending modes are present. The H/TiO_2 species produced from pyrolysis of H_2 by a hot W filament is always accompanied by fractions of a monolayer of inclined OH/TiO_2 species due to impurity H_2O adsorption.

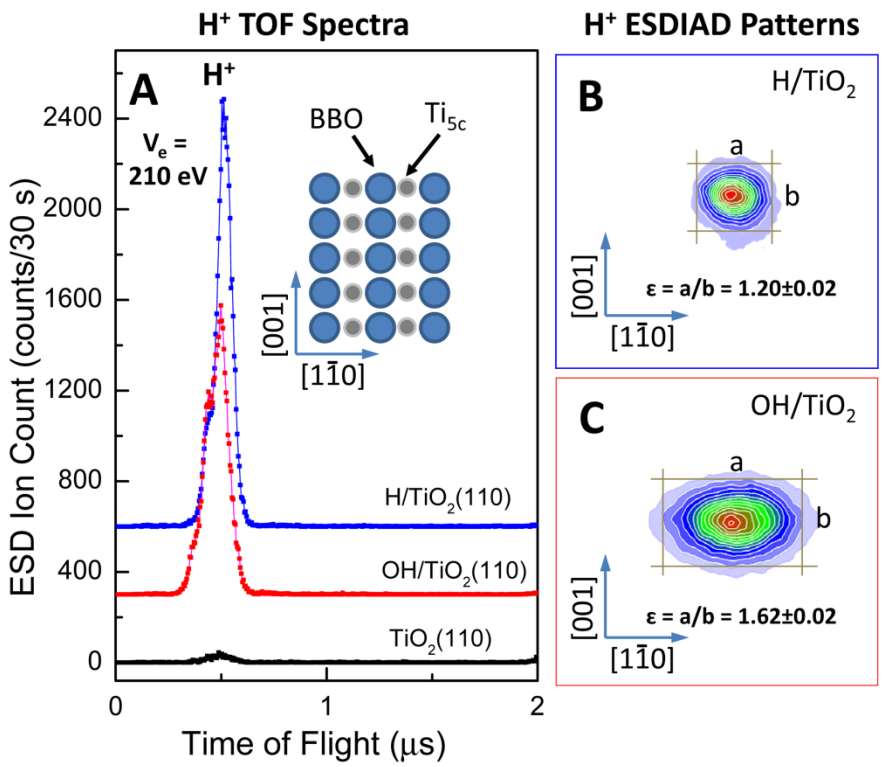

Figure 4.1: Electron stimulated desorption of H/TiO_2 and OH/TiO_2. (A). Time-of-flight spectra of H^+ produced by 210 eV electron bombardment on $TiO_2(110)$, $OH/TiO_2(110)$ and $H/TiO_2(110)$ surfaces. (B) and (C). H^+ ion angular distribution patterns on H/TiO_2 and OH/TiO_2 surfaces. In (B), the contribution of OH/TiO_2 is removed by thermal treatment of the surface based on the behavior shown in Figure 4.2.

The thermal properties of H/TiO_2 and OH/TiO_2 differ greatly as shown in Figure 4.2. Here we use the yield of H^+ by ESD for study of the two surface hydrogenic species. For H/TiO_2, depletion by heating in vacuum occurs up to ~350 K as shown in Figure 4.2A, followed by a fractional ML remaining coverage of OH/TiO_2 depletion above ~350 K. The OH is inadvertently added to the surface

during bombardment by atomic H from small quantities of H_2O produced in the ultrahigh vacuum chamber. When only H_2O is adsorbed, to produce only OH/TiO_2, the behavior of the OH/TiO_2 upon heating is shown in Figure 4.2B, indicating that OH/TiO_2 thermal depletion occurs only above ~350 K. From the data in Figure 4.2, we see that saturation coverage of H/TiO_2 above the background due to OH/TiO_2 gives about 19×10^3 H^+ counts/30 s, whereas the saturation coverage of OH/TiO_2 gives about 33×10^3 H^+ counts/30 s. These count rates are consistent with those measured by integration in Figure 4.1A. The thermal stability of OH/TiO_2 shown in Figure 4.2 exceeds that of H/TiO_2, showing that the two kinds of surface hydrogen differ chemically.

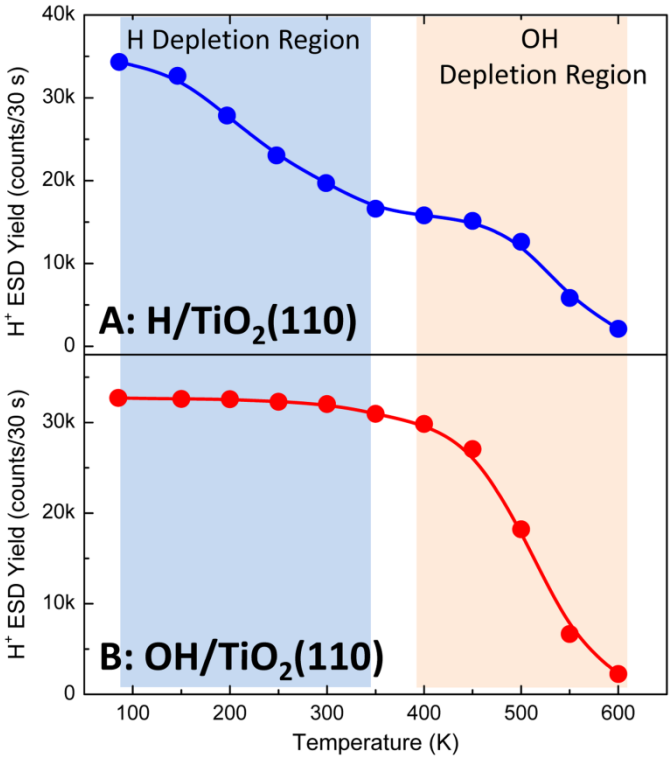

Figure 4.2: Thermal behavior of H/TiO_2 and OH/TiO_2 for desorption into vacuum.

The chemical difference between H/TiO_2 and OH/TiO_2 is also vividly demonstrated by comparing their sensitivity to electron stimulated desorption. Figure 4.3A shows the almost complete lack of sensitivity of OH/TiO_2 to electron stimulated desorption (V_e = 210 eV) at an electron flux $F_e = 6.25 \times 10^{10}$ e cm^{-2} s^{-1}. In contrast, for H/TiO_2, for F_e in the range $0.31–3.13 \times 10^{10}$ e cm^{-2} s^{-1}, a monotonically increasing and large rate of H depletion by ESD is observed. H/TiO_2 is very sensitive to electrons and responds both by ionization to produce H^+ and by the breaking of the H/TiO_2 bond by 210 eV electrons. Data like that shown in Figure 4.3A are combined

to show the H/TiO_2 exponential decay time during ESD. The exponential dependence in Figure 4.3B was used to derive the cross section of ESD of H/TiO_2, and a cross section value of $Q = 7.1 \times 10^{-14}$ cm^2 is found. This very large cross section indicates that multiple electronic events occur during 210 eV electron bombardment of the $TiO_2(110)$ surface and that the H atoms from the H/TiO_2 species desorb by excitation processes involving multiple charge carriers produced in the TiO_2 by 210 eV electron bombardment. In contrast to the very high cross section for H/TiO_2, the cross section for OH/TiO_2 is estimated to be only $\sim 10^{-20}$ cm^2, a more normal total ESD-cross section. This large contrast in total cross section for ESD of H from H/TiO_2 and from OH/TiO_2 is again indicative of the large chemical difference between the two kinds of bound H on the $TiO_2(110)$ surface.

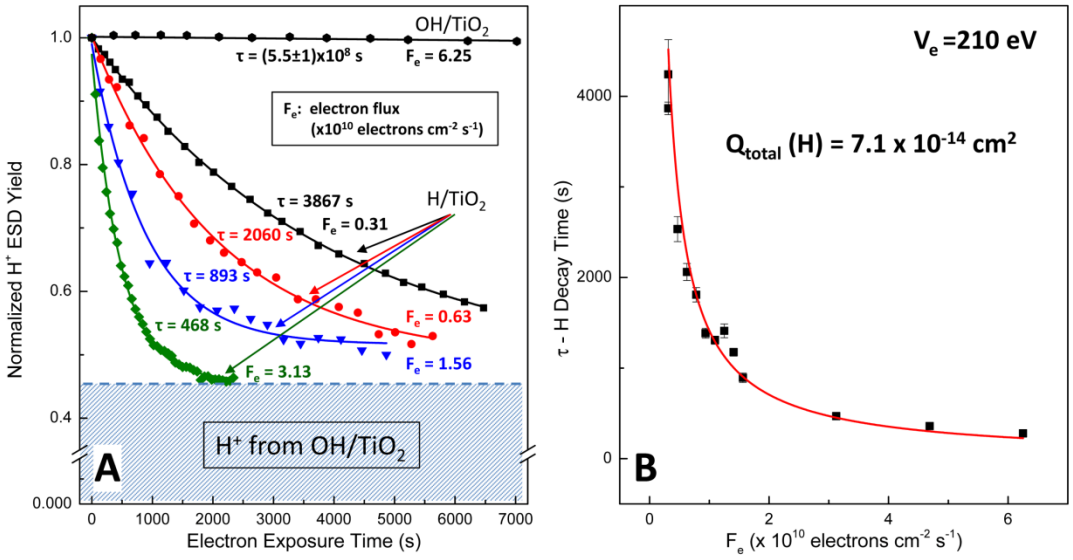

Figure 4.3: H/TiO_2- ESD cross section measurement.

The TOF-ESDIAD measurement technique also permits us to measure the influence of UV irradiation on the coverage of H/TiO_2 by monitoring the H^+-ESD yield during UV irradiation. Using (for analysis) only the ESD production of H^+ from H/TiO_2 (at $F_e = 6.25 \times 10^{10}$ e cm^{-2} s^{-1}, which is too small to cause significant damage in the measurements), it is seen that H/TiO_2 species are also able to be desorbed by UV photons of 3.4 ± 0.1 eV energy, just above the TiO_2 bandgap. Figure 4.4 shows the effect of UV irradiation on H/TiO_2. It may be seen that an exponential decay is observed, and that by ~ 5×10^{16} photons cm^{-2} exposure, all H/TiO_2 species have been desorbed by UV irradiation. A control experiment in the dark is negative. In addition, OH/TiO_2 is found to be insensitive to 3.4 eV photons. Figure 4.4 shows that about 50 ML of 3.4 eV photons are capable of completely removing the H/TiO_2 monolayer. The total photodesorption cross section (~10^{-16} cm^2) is ~10^{-3} that of

the ESD process caused by 210 eV electrons, as determined by the exponential fit. It is clear that H/TiO_2 is very sensitive to electronic excitation either by electrons or 3.4 eV photons, whereas OH/TiO_2 is orders of magnitude less capable of being desorbed or ionized by electrons or photons.

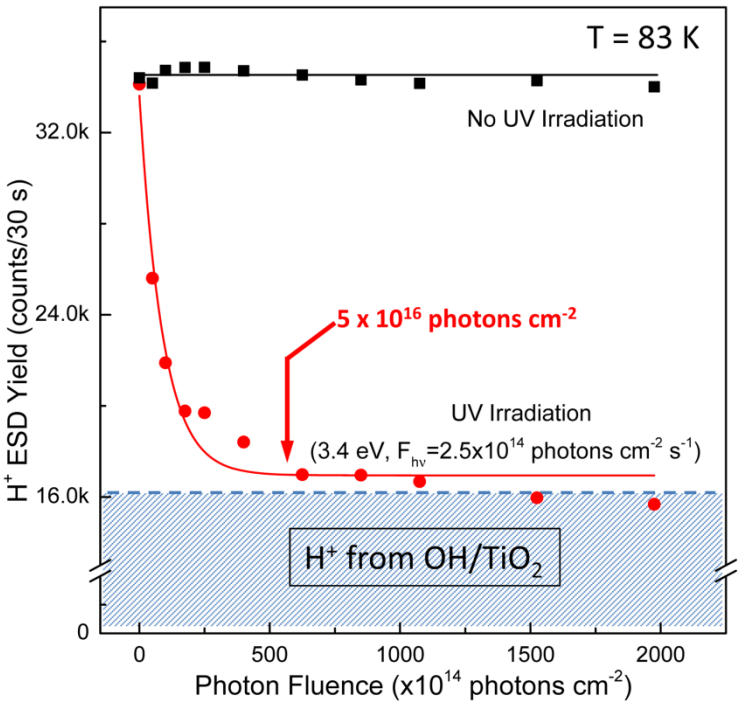

Figure 4.4: Photon stimulated desorption of H/TiO_2 with 3.4 eV photons.

The reversibility of H/TiO_2 adsorption and photodesorption was tested by cycles of atomic H adsorption, followed by photodesorption with the full spectrum of a 500 W Hg arc lamp ($h\nu < 5.1$ eV) employing an IR filter to eliminate crystal heating. In this work (Figure 4.5), the surface before the first cycle of atomic H adsorption is saturated by OH species by exposing to water at 320 K. From two cycles of atomic H adsorption, followed

by UV-induced H photodesorption, it was found that the addition and photodesorption of atomic H seems to be essentially reversible. OH/TiO_2 adsorption is essentially uninfluenced by UV excitation, allowing the reversibility studies to be accomplished without changing the OH/TiO_2 coverage.

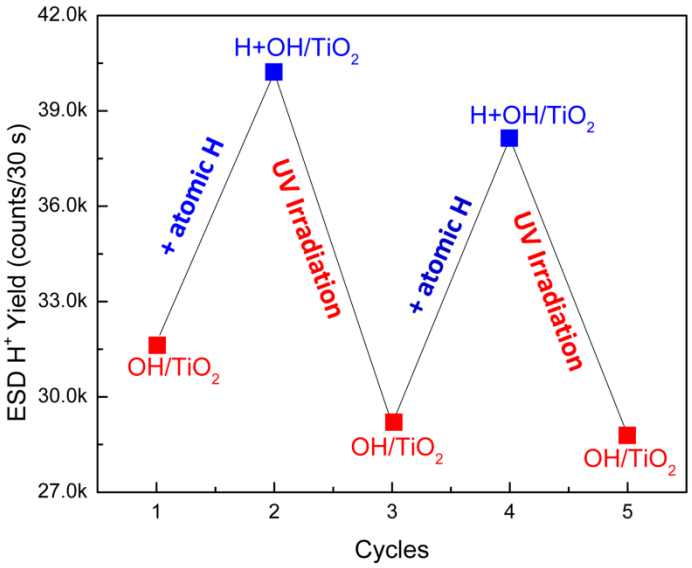

Figure 4.5: Reversible atomic H adsorption - UV photodesorption for H/TiO_2; H is adsorbed on top of a saturated OH/TiO_2 surface.

4.5 Summary and Future Directions

Chemically-bound hydrogen, H/TiO_2, on the $TiO_2(110)$ surface is produced by exposure to atomic H at 87 K. This chemisorbed hydrogen differs significantly in its physical and chemical properties from OH/TiO_2 species produced from H_2O adsorption.

The H/TiO_2 species produces a normal beam of H^+ upon electron stimulated desorption whereas OH/TiO_2 species produce inclined H^+ ESD beams. This indicates that H/TiO_2 is normally-bonded to its adsorption site, whereas OH/TiO_2 exhibits an inclined O-H bond in the $[1\bar{1}0]$ direction. It would be good to examine the vibrational dynamics of Ti-OH species to determine if the H^+-ESDIAD pattern elongation may be rationalized theoretically.

It is likely that H/TiO_2 is bound at Ti_{5c} sites between the rows of bridged O atoms that constitute the outer surface of $TiO_2(110)$. Therefore, future theoretical work of DFT calculations of the favorability of Ti_{5c}-H formation would be useful, as well as possible synergism between Ti_{5c}-H and neighboring Ti-OH species. Also, experimentally, studies have shown that CO[105] and CO_2[106] can bind at Ti_{5c} sites and thus they can be good candidates for studying the atomic H binding sites via TPD experiments.

H/TiO_2 is thermally less stable than OH/TiO_2. By ~ 350 K, H/TiO_2 has desorbed thermally as H_2 whereas OH/TiO_2 begins to desorb as H_2O only above ~ 350 K. Future theoretical work of DFT calculations of binding energies and activation energies for desorption from the site of adsorption would be helpful for H/TiO_2.

H/TiO_2 exhibits an extremely large cross section for ESD by 210 eV electrons. This must indicate that 210 eV electrons produce a large yield of e-h pairs in the TiO_2 substrate causing efficient H desorption.

H/TiO_2 is highly sensitive to UV photodesorption using radiation capable of bandgap

excitation. H/TiO_2 can be reversibly photodesorbed by UV and readsorbed using atomic H in the presence of a monolayer of OH/TiO_2 .

References

[1] A. Fujishima, K. Honda, *Nature* **1972,** *238*, 37.

[2] B. O'Regan, M. Grätzel, *Nature* **1991,** *353*, 737.

[3] X. Chen, S. S. Mao, *Chem. Rev.* **2007,** *107*, 2891-2959.

[4] O. K. Varghese, C. A. Grimes, *J. Nanosci. Nanotechnol.* **2003,** *3*, 277-293.

[5] D. C. Sorescu, W. A. Al-Saidi, K. D. Jordan, *J. Chem. Phys.* **2011,** *135*, 124701.

[6] R. Wang, K. Hashimoto, A. Fujishima, M. Chikuni, E. Kojima, A. Kitamura, M. Shimohigoshi, T. Watanabe, *Nature* **1997,** *388*, 431-432.

[7] T. Zubkov, D. Stahl, T. L. Thompson, D. A. Panayotov, O. Diward, J. T. Yates, Jr., *J. Phys. Chem. B* **2005,** *109*, 15454-15462.

[8] G. Lu, A. L. Linsebigler, J. T. Yates, Jr., *Chem. Rev.* **1995,** *95*, 735-758.

[9] U. Diebold, *Surf. Sci. Rep.* **2003,** *48*, 53-229.

[10] A. Fujishima, X. Zhang, D. A. Tryk, *Surf. Sci. Rep.* **2008,** *63*, 515-582.

[11] Z. Zhang, J. Lee, J. T. Yates, Jr., R. Bechstein, E. Lira, J. Ø. Hansen, S. Wendt, F. Besenbacher, *J. Phys. Chem. C* **2010,** *114*, 3059-3062.

[12] P. J. Møller, M. -C. Wu, *Surf. Sci.* **1989,** *224* (265-276).

[13] C. Sánchez-Sánchez, J. A. Martín-Gago, M. F. López, *Surf. Sci.* **2013,** *607* (159-163).

[14] S. Wendt, J. Matthiesen, R. Schaub, E. K. Vestergaard, E. Lægsgaard, F. Besenbacher, B. Hammer, *Phys. Rev. Lett.* **2006,** *96*, 066107.

[15] M.A. Henderson, W.S. Epling, C.H.F. Peden, C.L. Perkins, *J. Phys. Chem. B* **2003,** *107*, 534-545.

[16] C. L. Pang, R. Lindsay, G. Thronton, *Chem. Sov. Rev.* **2008,** *37* (2328-2353).

[17] M. A. Henderson, *Langmuir* **1996,** *12*, 5093-5098.

[18] M. A. Henderson, *Surf. Sci.* **1998,** *400*, 203-219.

[19] L. M. Liu, B. McAllister, H. Q. Ye, P. Hu, *J. Am. Chem. Soc.* **2006,** *128*, 4017-4022.

[20] D. C. Sorescu, W. J. Lee, A. Al-saidi, K. D. Jordan, *J. Chem. Phys.* **2012,** *137*, 074704.

[21] S. C. Li, P. Jacobson, S. L. Zhao, X. Q. Gong, U. Diebold, *J. Phys. Chem. C* **2012,** *116*, 1887-1891.

[22] Z. Zhang, O. Bondarchuk, B. D. Kay, J. M. White, Z. Dohnalek, *J. Phys. Chem. B* **2006,** *110*, 21840-21845.

[23] M.B. Hugenschmidt, L. Gamble, C.T. Campbell, *Surf. Sci.* **1994,** *302*, 329-340.

[24] I. M. Brookes, C. A. Muryn, G. Thornton, *Phys. Rev. Lett.* **2001,** *87*, 266103.

[25] R. Schaub, P. Thostrup, N. Lopez, E. Laegsgaard, I. Stensgaard, J. K. Nørskov, F. Besenbacher, *Phys. Rev. Lett.* **2001,** *87* (266104).

[26] S. Wendt, R. Schaub, J. Matthiesen, E. K. Vestergaard, E. Wahlström, M. D. Rasmussen, P. Thostrup, L. M. Molina, E. Laegsgaard, I. Stensgaard, B. Hammer, F. Besenbacher, *Surf. Sci.* **2005,** *598*, 226-245.

[27] M. A. Henderson, *Surf. Sci.* **1996,** *355*, 151-166.

[28] N. G. Petrik, G. A. Kimmel, *Phys. Rev. Lett.* **2007,** *99*, 196103.

[29] J. Lee, D. C. Sorescu, X. Deng, K. D. Jordan, *J. Phys. Chem. Lett.* **2012,** *4*, 53-57.

[30] J. -M. Pan, B. L. Maschhoff, U. Diebold, T. E. Madey, *J. Vac. Sci. Technol. A* **1992,** *10*, 2470.

[31] W. Unterberger, T. J. Lerotholi, E. A. Kroger, M. J. Knight, D. A. Duncan, D. Kreikemeyer-Lorenzo, K. A. Hogan, D. C. Jackson, R. Wlodarczyk, M. Sierka, J. Sauer, D. P. Woodruff, *Phys. Rev. B* **2011,** *84*, 115461.

[32] D. A. Panayotov, J. T. Yates, Jr., *J. Phys. Chem. C* **2007,** *111*, 2959-2964.

[33] X. -L. Yin, M. Calatayud, H. Qiu, Y. Wang, A. Birkner, C. Minot, Ch. Wöll, *ChemPhysChem* **2008,** *9*, 253-256.

[34] Y. Du, N. G. Petrik, N. A. Deskins, Z. Wang, M. A. Henderson, G. A. Kimmel, I. Lyubinetsky, *Phys. Chem. Chem. Phys.* **2012,** *14*, 3066-3074.

[35] S. Suzuki, K. Fukui, H. Onishi, Y. Iwasawa, *Phys. Rev. Lett.* **2000,** *84*, 2156-2159.

[36] M. C. Torquemada, J. L. de Segovia, *J. Vac. Sci. Technol. A* **1994,** *12*, 2318-2322.

[37] C. L. Greenwood, E. M. Williams, G. Thornton, S. L. Bennett, E. Roman, J. L. de Segovia, M. C. Torquemada, *Surf. Sci.* **1993,** *287*, 386-390.

[38] J. L. de Segovia, M. C. Torquemada, E. Roman, *J. Phys.: Condens. Matter* **1993,** *5*, A139-A142.

[39] I. Cocks, Q. Guo, E. M. Williams, *Surf. Sci.* **1997,** *390*, 119-125.

[40] M. C. Torquemada, J. L. de Segovia, *Vacuum* **1995,** *46*, 1219-1222.

[41] M. C. Torquemada, J. L. de Segovia, E. Roman, *Surf. Sci.* **1995,** *337*, 31-39.

[42] M. A. Henderson, S. Otero-Tapia, M. E. Castro, *Surf. Sci.* **1998,** *412-13*, 252-272.

[43] B. Yakshinskly, M. Akbulut, T. E. Madey, *Surf. Sci.* **1997,** *390*, 132-139.

[44] V. N. Ageev, S. Solovev, *Phys. Solid State* **2000,** *42*, 2159-2163.

[45] Q. Guo, I. Cocks, E. M. Williams, *J. Chem. Phys.* **1997,** *106*, 2924-2931.

[46] U. Diebold, T. E. Madey, *J. Vac. Sci. Technol. A* **1992,** *10*, 2327.

[47] C. D. Lane, N. G. Petrik, T. M Orlando, G. A. Kimmel, *J. Phys. Chem. C* **2007,** *111*, 16319-16329.

[48] C. D. Lane, N. G. Petrik, T. M Orlando, G. A. Kimmel, *J. Chem. Phys.* **2007,** *127*, 224706.

[49] J. Lee, Z. Zhang, J. T. Yates, Jr., *Phys. Rev. B* **2009,** *79*, 081408.

[50] Z. Zhang, J. T. Yates, Jr., *J. Phys. Chem. Lett.* **2010,** *1*, 2185-2188.

[51] Z. Zhang, J. T. Yates, Jr., *J. Phys. Chem. C* **2010,** *114*, 3098-3101.

[52] R. D. Ramsier, J. T. Yates, Jr., *Surf. Sci. Rep.* **1991,** *12*, 243-378.

[53] T. E. Madey, D. E. Ramaker, R. Stockbauer, *Ann. Rev. Phys. Chem.* **1984,** *35*, 215-240.

[54] D. Menzel, *Nucl. Instr. and Meth. in Phys. Res. B* **1995,** *101*, 1-10.

[55] P. A. Redhead, *Vacuum* **1997,** *48*, 585-596.

[56] M. L. Knotek, P. J. Feibelman, *Phys. Rev. Lett.* **1978,** *40*, 964.

[57] Z. Zhang, K. Cao, J. T. Yates, Jr., *J. Phys. Chem. Lett.* **2013,** *4*, 674-679.

[58] http://www.newport.com/Flood-Exposure-Sources/378214/1033/info.aspx.

[59] J. T. Yates, Jr., *Experimental Innovations in Surface Science*. Springer-Verlag: 1997; p 604.

[60] T. L. Thompson, J. T. Yates, Jr., *Chem. Rev.* **2006,** *106*, 4428-4453.

[61] M.A. Henderson, *Surf. Sci. Reports* **2011,** *66*, 185-297.

[62] G. Lu, A. L. Linsebigler, J. T. Yates, Jr., *J. Phys. Chem.* **1994,** *98*, 11733-11738.

[63] O. Bikondoa, C. L. Pang, R. Ithnin, C. A. Muryn, H. Onishi, G. Thornton, *Nat. Mater.* **2006,** *5*, 189-192.

[64] S. Wendt, P. T. Sprunger, E. Lira, G. K. H. Madsen, Z. Li, J. Ø. Hansen, J. Matthiesen, A. Blekinge-Rasmussen, E. Lægsgaard, B. Hammer, F. Besenbacher, *Science* **2008,** *320*, 1755-1759.

[65] P. Krüger, J. Jupille, S. Bourgeois, B. Domenichini, A. Verdini, L. Floreano, A. Morgante, *Phys. Rev. Lett.* **2012,** *108*, 126803.

[66] C. M. Yim, C. L. Pang, G. Thornton, *Phys. Rev. Lett.* **2010,** *104*, 036806.

[67] K. Mitsuhara, M. Okumura, A. Visikovskiy, M. Takizawa, Y. Kido, *J. Chem. Phys.* **2012,** *136*, 124707.

[68] R. L. Kurtz, R. Stockbauer, T. E. Madey, E. Roman, J. L. de Segovia, *Surf. Sci.* **1989,** *218*, 178-200.

[69] N. G. Petrik, Z. Zhang, Y. Du, Z. Dohnalek, I. Lyubinetsky, G. A. Kimmel, *J. Phys. Chem. C* **2009,** *113*, 12407-12411.

[70] L. M. Liu, P. Crawford, P. Hu, *Prog. Surf. Sci.* **2009,** *84*, 155-176.

[71] Z. Dohnalek, I. Lyubinetsky, R. Rousseau, *Prog. Surf. Sci.* **2010,** *85*, 161-205.

[72] C. Di Valentin, G. Pacchioni, A. Selloni, *J. Phys. Chem. C* **2009,** *113*, 20543-20552.

[73] A. G. Thomas, W. R. Flavell, A. R. Kumarasinghe, A. K. Mallick, D. Tsoutsou, G. C. Smith, R. Stockbauer, S. Patel, M. Gratzel, R. Hengerer, *Phys. Rev. B* **2003,** *67*, 035110.

[74] P. Krüger, S. Bourgeois, B. Domenichini, H. Magnan, D. Chandesris, P. Le Fèvre, A. M. Flank, J. Jupille, L. Floreano, A. Cossaro, A. Verdini, A. Morgante, *Phys. Rev. Lett.* **2008,** *100*, 055501.

[75] E. Serwicka, M. W. Schlierkamp, R. N. Schindler, *Z. Naturforsch.* **1981,** *36a*, 226-232.

[76] S. Chrétien, H. Metiu, *J. Phys. Chem. C* **2011,** *115*, 4696-4705.

[77] N. A. Deskins, R. Rousseau, M. Dupuis, *J. Phys. Chem. C* **2011,** *115*, 7562-7572.

[78] T. Shibuya, K. Yasuoka, S. Mirbt, B. Sanyal, *J. Phys.: Condens. Matter* **2012,** *24*, 435504.

[79] P. M. Kowalski, M. F. Camellone, N. N. Nair, B. Meyer, D. Marx, *Phys. Rev. Lett.* **2010,** *105*, 146405.

[80] A. C. Papageorgiou, N. S. Beglitis, C. L. Pang, G. Teobaldi, G. Cabailh, Q. Chen, A. J. Fisher, W. A. Hofer, G. Thronton, *Proc. Natl. Acad. Sci. USA* **2010,** *107*, 2391-2396.

[81] T. Minato, Y. Sainoo, Y. Kim, H. S. Kato, K. Aika, M. Kawai, J. Zhao, H. Petek, T. Huang, W. He, B. Wang, Z. Wang, Y. Zhao, J. L. Yang, J. G. Hou, *J. Chem. Phys.* **2009,** *130*, 124502.

[82] C. Di Valentin, G. Pacchioni, A. Selloni, *Phys. Rev. Lett.* **2006,** *97*, 166803.

[83] J. Ahner, D. Mocuta, J.T. Yates, Jr., *J. Vac. Sci. Technol. A* **1999,** *17*, 2333-2338.

[84] R. T. Zehr, M. A. Henderson, *Surf. Sci.* **2008,** *602*, 1507-1516.

[85] B. Bonelli, M. Cozzolino, R. Tesser, M. Di Serio, M. Piumetti, E. Garrone, E. Santacesaria, *J. Catal.* **2007,** *246*, 293-300.

[86] T. Bezrodna, G. Puchkovska, V. Shimanovska, I. Chashechnikova, T. Khalyavka, J. Baran, *Appl. Surf. Sci.* **2003,** *214*, 222-231.

[87] J. Lee, Z. Zhang, J.T. Yates, Jr., *Phys. Rev. B* **2009,** *79*, 081408(R).

[88] A. T. Paxton, L. Thiên-Nga, *Phys. Rev. B* **1998,** *57*, 1579-1584.

[89] S.-i. Tanaka, K. Mase, S.-i. Nagaoka, *Surf. Sci.* **2004,** *572*, 43-58.

[90] U. Diebold, T. E. Madey, *Phys. Rev. Lett.* **1994,** *72*, 1116-1119.

[91] M. Akbulut, N. J. Sack, T. E. Madey, *J. Chem. Phys.* **1995,** *103*, 2202-2215.

[92] O. Dulub, M. Batzill, S. Solovev, E. Loginova, A. Alchagirov, T. E. Madey, U. Diebold, *Science* **2007,** *317*, 1052-1056.

[93] L. R. Merte, G. Peng, R. Bechstein, F. Rieboldt, C. A. Farberow, L. C. Grabow, W. Kudernatsch, S. Wendt, E. Lægsgaard, M. Mavrikakis, F. Besenbacher, *Science* **2012,** *336*, 889-893.

[94] D. A. Panayotov, S. P. Burrows, J. T. Yates, Jr., J. R. Morris, *J. Phys. Chem. C* **2011,** *115*, 22400-22408.

[95] S. Khoobiar, *J. Phys. Chem.* **1964,** *68*, 411-412.

[96] F. Boccuzzi, A. Chiorino, G. Ghiotti, E. Guglielminotti, *Langmuir* **1989,** *5*, 66-70.

[97] M. D. Marcinkowski, A. D. Jewell, M. Stamatakis, M. B. Boucher, E. A. Lewis, C. J. Murphy, G. Kyriakou, E. C. H. Sykes, *Nat. Mater.* **2013,** *12*, 523-528.

[98] A. Al-Mahboob, E. Muller, A. Karim, J. T. Muckerman, C. V. Ciobanu, P. Sutter, *J. Am. Chem. Soc.* **2012,** *134*, 10381-10384.

[99] X. Chen, L. Liu, P. Y. Yu, S. S. Mao, *Science* **2011,** *331*, 746-750.

[100] L. Zhang, R. Persaud, T. E. Madey, *Phys. Rev. B* **1997,** *56*, 10549-10557.

[101] X. Lai, T. P. St Clair, M. Valden, D. W. Goodman, *Prog. Surf. Sci.* **1998,** *59*, 25-52.

[102] V. A. Bondzie, S. C. Parker, C.T. Campbell, *Catal. Lett.* **1999,** *63*, 143-151.

[103] F. Cosandey, T. E. Madey, *Surf. Rev. Lett.* **2001,** *8*, 73-93.

[104] M. A. Henderson, *Surf. Sci.* **1999,** *419*, 174-187.

[105] A. L. Linsebigler, G. Lu, J. T. Yates, Jr., *J. Phys. Chem.* **1995,** *103*, 9438-9443.

[106] T. L. Thompson, O. Diwald, J. T. Yates, Jr., *J. Phys. Chem. B* **2003,** *107*, 11700-11704.

Appendix

Appendix A: UV-Vis Spectra of Selected Longpass Filters and Bandpass Filters

The longpass filters and bandpass filters were tested using a Hewlett-Packard 8452A Diode Array Spectrophotometer. Some selected spectra are shown in Figure A1 and A2.

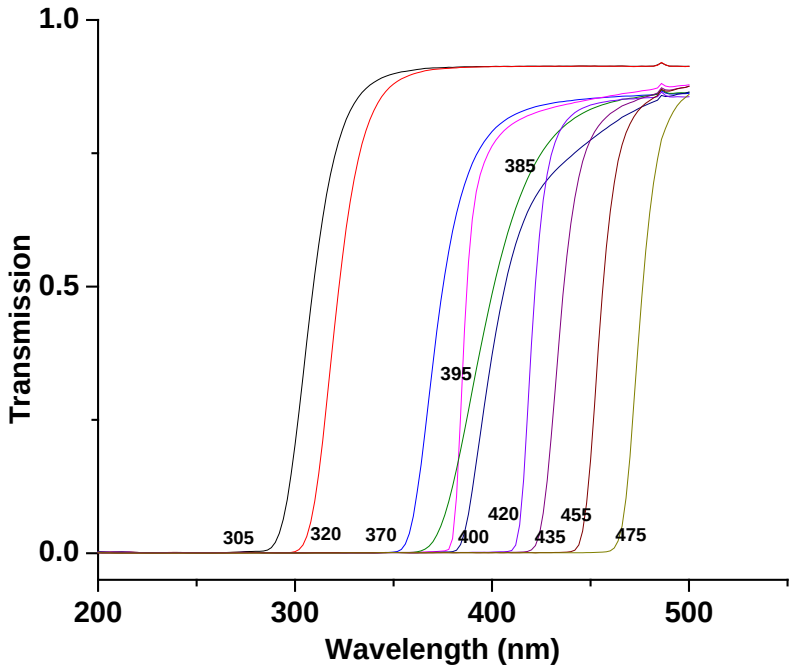

Figure A1: UV-Vis spectra of longpass filters; cut-off wavelengths are marked respectively in the figure.

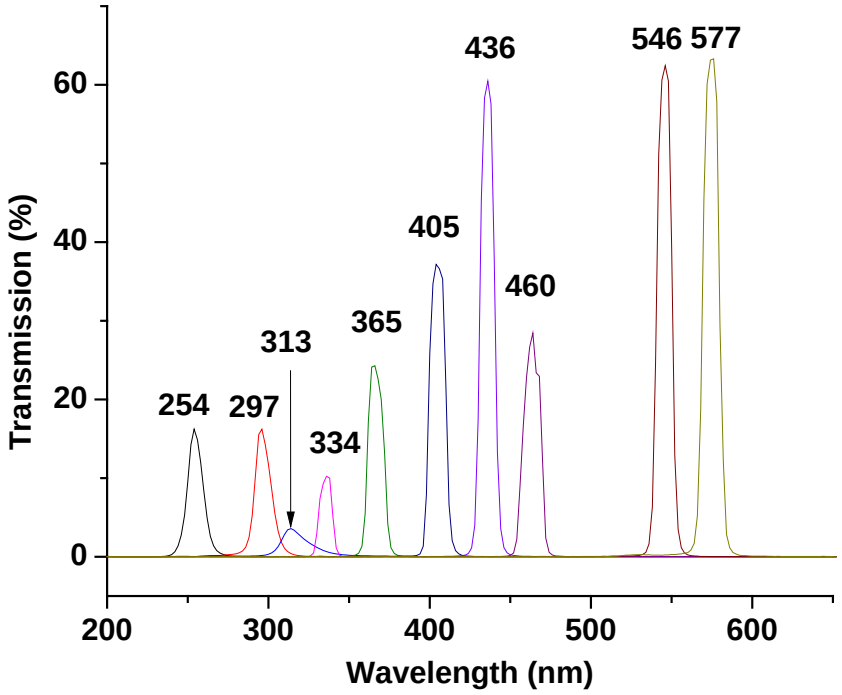

Figure A2: UV-Vis spectra of bandpass filters; center wavelengths are marked respectively in the figure.